Results in Chemistry 4 (2022) 100480

Contents lists available at ScienceDirect

Results in Chemistry

journal homepage: www.sciencedirect.com/journal/results-in-chemistry

Photocatalytic degradation of malachite green dye using nitrogen/sodium/iron-TiO_2 nanocatalysts

A.T. Amigun [a,b], F.A. Adekola [b], J.O. Tijani [c,d], S. Mustapha [c,d,*]

[a] Department of Chemical and Geological Sciences, Al-Hikmah University, Ilorin PMB1601, Nigeria
[b] Department of Industrial Chemistry, University of Ilorin, PMB 1515 Ilorin, Nigeria
[c] Department of Chemistry, Federal University of Technology, Bosso Campus, Minna PMB 65, Nigeria
[d] Nanotechnology Research Group, African Centre of Excellence on Food Safety and Mycotoxins, Federal University of Technology, P.M.B 65, Bosso, Minna, Niger State, Nigeria

ARTICLE INFO

Keywords:
Green synthesis
N/Na/Fe-TiO_2
Malachite green dye
Photocatalysis

ABSTRACT

Enhanced visible light-responsive TiO_2 modified with nitrogen, sodium, and iron was synthesized using an integration of green synthesis and wet impregnation method. The prepared nanocatalysts were characterized using some analytical tools like UV–visible spectrometry (UV–visible), photoluminescence (PL), High-resolution transmission electron microscopy, X-ray diffraction, Brunauer–Emmett–Teller N_2 adsorption–desorption process, X-ray photoelectron spectroscopy, and Fourier-transform infrared spectroscopy, The photocatalytic activity of N/Na/Fe–TiO_2 and bared TiO_2 for the degradation of Malachite green (MG) dye in aqueous solution under visible light was investigated. The response surface methodology (RSM) based on Box Benhken Design was used to evaluate the interaction between three important independent variables (reaction time, catalyst dosage, and dye solution pH). The XRD results of the prepared samples showed that the crystal phase was anatase irrespective of the modifiers. The BET surface areas of the tri-doped TiO_2 nanocatalysts (80.165 m^2/g) were higher than the undoped TiO_2 (10.25 m^2/g). XPS analysis confirmed the existence of Ti in + 4 oxidation states with or without the dopants. The MG removal efficiency was pH and catalyst dosage-dependent, and maximum MG degradation (96.57 %) was obtained using N/Na/Fe tri-doped TiO_2 nanocatalyst under optimum experimental conditions of 0.11 g catalyst dosage, 25.83 min reaction time, and pH of 9.89. The N/Na/Fe-TiO_2 nanocatalyst was reusable for up to 5 cycles without significant loss of photocatalytic activity.

Introduction

The discharges of industrial wastewater, particularly wastewater from industrial textile industries, into the aquatic environment have been associated with severe environmental and health problems due to various non-biodegradable dyes and biological contaminants. [11]. Synthetic dyes like malachite green (MG) are a cationic triphenylmethane dye highly persistent and carcinogenic hazardous chemical often used in the dyeing operation [7,35]. As a result of the shortcomings in terms of high cost, high energy consumption, and toxic secondary waste generation associated with conventional dye removal approaches, researchers have focused on providing lasting solutions to industrial wastewater treatment based on the complement of the conventional methods with highly efficient and sustainable water treatment methods [53]. Advanced oxidation processes involving the generation of highly chemical oxidants have shown effective degradation of a wide range of organic contaminants in polluted water [48]. Advanced oxidation processes, such as heterogeneous photocatalysis, can be achieved by combining a titania-based catalyst with UV–visible light, and it is more effective in decomposing recalcitrant complex organic pollutants than conventional methods [48].

TiO_2 nanoparticles are widely studied among semiconductor metal oxides due to their exceptional properties such as ease of production, strong catalytic activity, low cost, chemical inertness, high efficiency, and long-term stability in an aqueous medium [3]. Studies have shown that the TiO_2 anatase phase with a large surface area, high crystallinity, and nano-scaled crystallite size usually exhibits a higher level of photocatalytic activity and possesses hydrophilic surfaces than the rutile phase [45]. However, several limitations are associated with using TiO_2 photocatalysts and ultraviolet (UV) activation and recombining the

* Corresponding author at: Department of Chemistry, Federal University of Technology, Bosso Campus, Minna PMB 65, Nigeria.
E-mail address: saheedmustapha09@gmail.com (S. Mustapha).

https://doi.org/10.1016/j.rechem.2022.100480
Received 4 May 2022; Accepted 12 August 2022
Available online 17 August 2022

Table 1
Independent variables with coded factors and levels for optimization of N/Na/Fe tri-doped TiO_2 nanocatalysts.

Coded Factors	Independent Variable	Range and Level		
		−1 (low)	0 (median)	1 (high)
A	Contact Time (min)	5	17.5	30.00
B	Catalyst Dosage (g)	0.1	0.15	0.2
C	pH	3	6.5	10.00

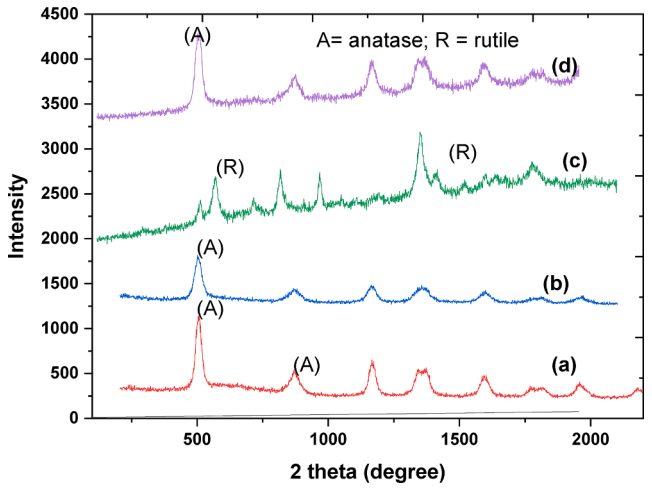

Fig. 1. XRD patterns of (a) pure TiO_2 (b) Na-TiO_2 (c) (2:1) N/Fe-TiO_2, (d) N/Na/Fe-TiO_2 TiO_2 annealed at 550 °C for 2 h.

generated electron-hole pairs [19]. Notably, modifications of TiO_2 photocatalysts through metal and non-metal ion-implanted TiO_2, metal (Fe, Na, Co, and La) or non-metal (B, C, N, S, and F), doping and co-doping (Fe and N, B and C), coating dye on TiO_2 surface, noble metal deposition and semiconductor coupling are effective strategies to avoid fast electron-hole recombination and also the extension of absorption threshold of TiO_2 towards visible light spectrum [25]. Vaiano et al. [50] reported N-TiO_2 nanoparticles with high catalytic properties to remove crystal violet dye. Ag-N co-doped TiO_2 nanoparticles were developed to photodegrade methylene blue dye of 20 ppm in 30 min of visible light exposure [57]. Masae et al. [29] synthesized sodium doped TiO_2 photocatalyst via a sol–gel method and the nanoparticle produced exhibited a higher photoactivity than pure TiO_2 films. They also realized that the high amount of doped Na promoted the formation of basic sites on the surface of TiO_2.

Recent studies on multi-doped TiO_2 have fast-tracked the interest of researchers more than single ion-doped TiO_2 studies because of the synergistic effect produced by the non-metal and metal co-doped system [14]. Both metals and non-metals have proven to be effective in introducing a mid-gap energy state in the TiO_2 energy levels, thereby increasing the surface area of its photocatalytic activities [24]. For the synthesis of multiple-doped titanium dioxide, several synthesis routes like implantation, sputtering, ball mill, solvothermal, and sol–gel methods have been adopted[44].

Green synthesis, which involves using plant extracts or microorganisms to replace toxic commercial reducing agents, has demonstrated researchers to be far superior to other approaches [52]. Secondary metabolites (phytochemicals) found in plant extracts act as a reducing and capping agent and help stabilize the crystalline phases and the size control of the synthesized nanoparticles [26]. In addition to the green synthesis route, the hydrothermal treatment route has also been recognized as an environmentally friendly process. The route offers a promising approach owing to its numerous advantages like low reaction

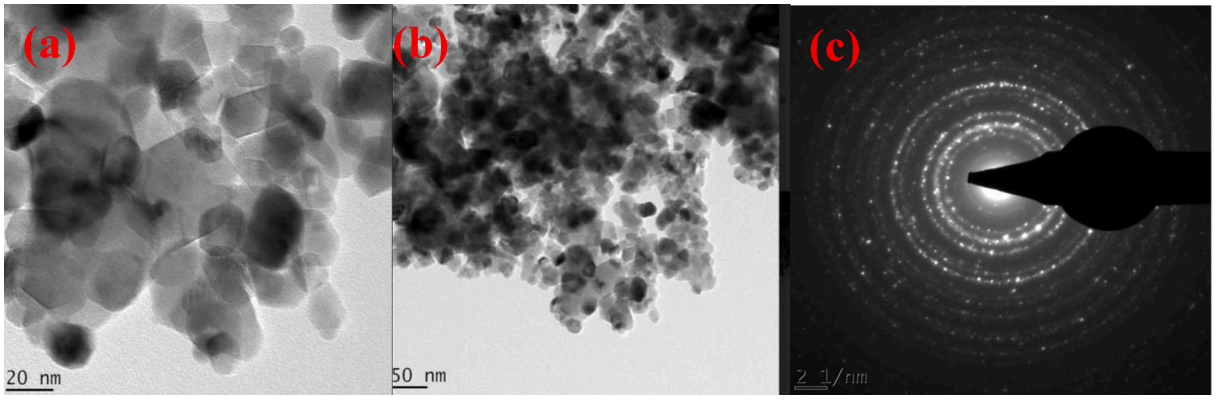

Fig. 2. (a) high (b) low HRTEM micrograph for pure TiO_2.

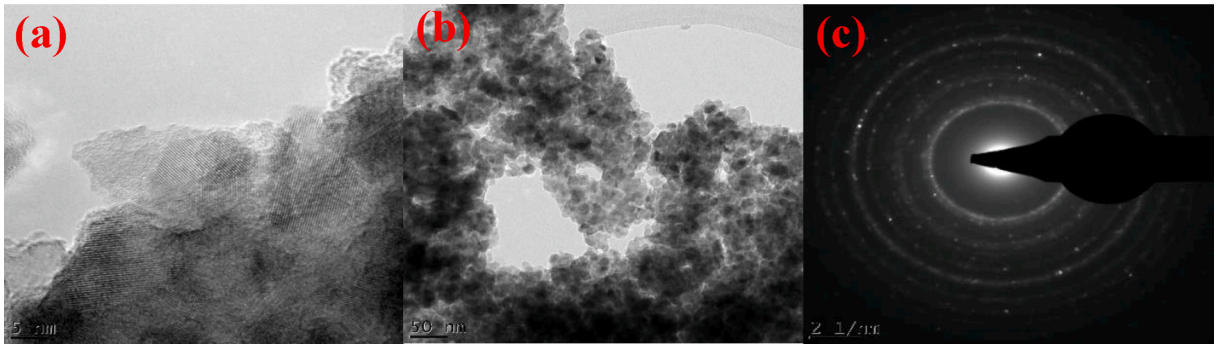

Fig. 3. (a) high (b) low HRTEM micrograph for (4:1) N/Fe co-doped TiO_2 nanocatalyst (c) SAED image.

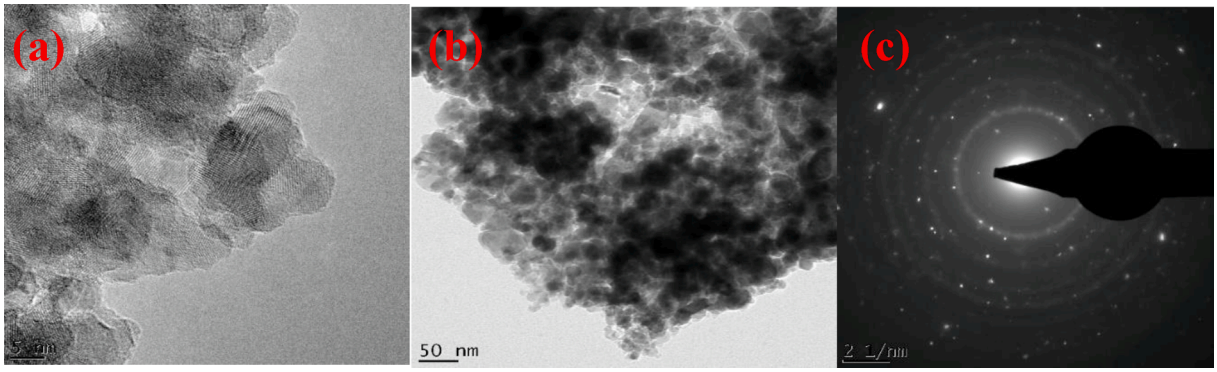

Fig. 4. (a) high (b) low HRTEM micrograph for (2:1:1) N/Na/Fe tri-doped TiO_2 nanocatalyst (c) SAED image.

Table 2
BET results of undoped and doped TiO_2 nanocatalysts.

Samples	Particle size (nm)	Surface area (m^2/g)	Pore size (nm)	Pore volume (cm^3/g)
Na-TiO_2	9.90 (A)	40.43	3.604	0.114
(4:1) N/Fe-TiO_2	25.06 (R)	27.487	1.056	0.087
(2:1:1) N/Na/Fe/Na-TiO_2	22.05 (R)	80.16	5.299	0.123
Pure TiO_2	6.95 (A)	10.25	4.086	0.096

temperature to produce nanocatalyst with reduced aggregation, high surface area, narrow particle size distribution, and well-defined unique morphology [1]. Vernonia *amygdalina*, also known as a bitter leaf, is a pantropical plant in the Asteraceae family with a small shrub of 2–5 m. The stem is rough, with young branches and petiolate green leaves measuring about 6 mm across. *Vernonia amygdalina* leaf extract has been shown to contain phytochemical components such as alkaloids, saponins, tannins, and phenols. Secondary metabolites (phytochemicals) found in plant extracts function as a reducing and capping agent in synthesizing TiO_2 nanoparticles [15]. Several factors influenced the morphology of the produced multiple-doped TiO_2 nanoparticles during the synthesis process. These factors include the pH of a solution, the calcination temperature, precursor concentration, aging time, chelating agent, the kinetics of precursor analysis, and catalyst dosage [6]. Aside from the morphology and composition of the photocatalysts, a variety of other parameters (pH, effluent concentration, catalyst dosage, temperature, light intensity, and contact time) can all impact the efficiency of the photocatalytic degradation process.

In general, doping with a sodium ion with a large ionic radius (1.02 Å) in the host TiO_2 lattice (0.68 Å) results in crystal structure strain. This lattice strain is compensated for by forming oxygen vacancies, which increases the adsorption of hydroxyl groups. Furthermore, Fe^{3+} with a half-filled electronic configuration could close the energy gap by forming new impurity energy levels, effectively improving charge carrier transport properties. Doping the TiO_2 lattice with nitrogen, which has a lower electronegativity than oxygen, causes the valence band of 2p-orbital levels to shift upward, resulting in a narrower bandgap. The issue with Fe dopant is that it acts as a charge carrier recombination center, inhibiting TiO_2 photocatalytic activity. However, these shortcomings could be averted via a combination of iron, sodium, and non-metals like nitrogen to improve the photocatalytic activities of TiO_2 nanocatalyst. The green synthesis of Na/Fe/N/TiO_2 nanocomposites will focus on exploring the superior photocatalytic activity in the ternary composites.

It is critical to optimize photocatalytic degradation processes based on these parameters for the determination of the maximum potential of the photocatalyst. Traditionally, optimizing a chemical process entails studying the effects of variables that affect its final result in isolation, referred to as the one factor at a time (OFAT) method [53]. This method is time-consuming, wasteful of materials and energy, and may be incorrect because it does not explain the interactions of the independent variables and the output [32]. As a result, an appropriate optimization approach response surface methodology (RSM) based on Box Behnken Design (BBD) was more cost-effective because it requires fewer experiments while still providing an accurate output prediction. To the greatest of our knowledge, there has been little or no research on the synergetic effect of N (non-metal), Na (alkali metal), and Fe (transition metal) on the crystal lattice of TiO_2 and its photocatalytic property on malachite green dye. Therefore, the current research aims to prepare *N*-Na-Fe tri-doped TiO_2 nanocatalysts and is the first study on its photocatalytic activities on malachite green dye.

Materials and method

Materials

The reagents used in this study were analytical grade. Titanium(IV) isopropoxide ($Ti[OCH(CH_3)_2]_4 \geq 97$ %), malachite green dye ($C_{23}H_{25}ClN_2$), sodium nitrate ($NaNO_3$, ≥ 99 %), ammonium nitrate ($NH_4NO_3 \geq 98$ %), sodium hydroxide, (NaOH, 98 %), iron(III) chloride hexahydrate ($FeCl_3{\cdot}6H_2O$, ≥ 97 %) and hydrochloric acid (HCl, 37 %) were purchased from Sigma Aldrich with a percentage in the range of 95–99.8 %.

Collection and pretreatment of Vernonia amygdalina

The leaves of *Vernonia amgydalina* were obtained from a local market in Ilorin, Kwara State, North Central, Nigeria. A plant biologist from Al-Hikmah University, Department of Microbiology, Faculty of Natural and Applied Sciences, Ilorin, Nigeria, validated the identification of the plant. Before being pulverized with a mortar and pestle, the leaves were washed and air-dried for two weeks. The powdered materials were kept in an airtight container for further research.

Preparation of Vernonia amgydalina leaves extract

A 250 cm^3 conical flask containing 200 cm^3 of sterile distilled water was filled with 20 g of powdered sample. The mixture was boiled for 30 min, and the extract was allowed to cool at room temperature before being filtered using Whatman No. 1 filter paper. The filtrate was placed in a refrigerator to be used in future experiments. This extract was used as a capping and stabilizing agent for the TiO_2 nanoparticles.

Preparation of TiO_2 photocatalyst

Green synthesis of TiO_2 nanoparticles

The green synthesis route reported by Goutam et al. [16] was used in this study. In a typical experiment, 60 cm^3 of *Vernonia amygdalina* aqueous extract was measured into a 250 cm^3 beaker, 12 cm^3 of de-

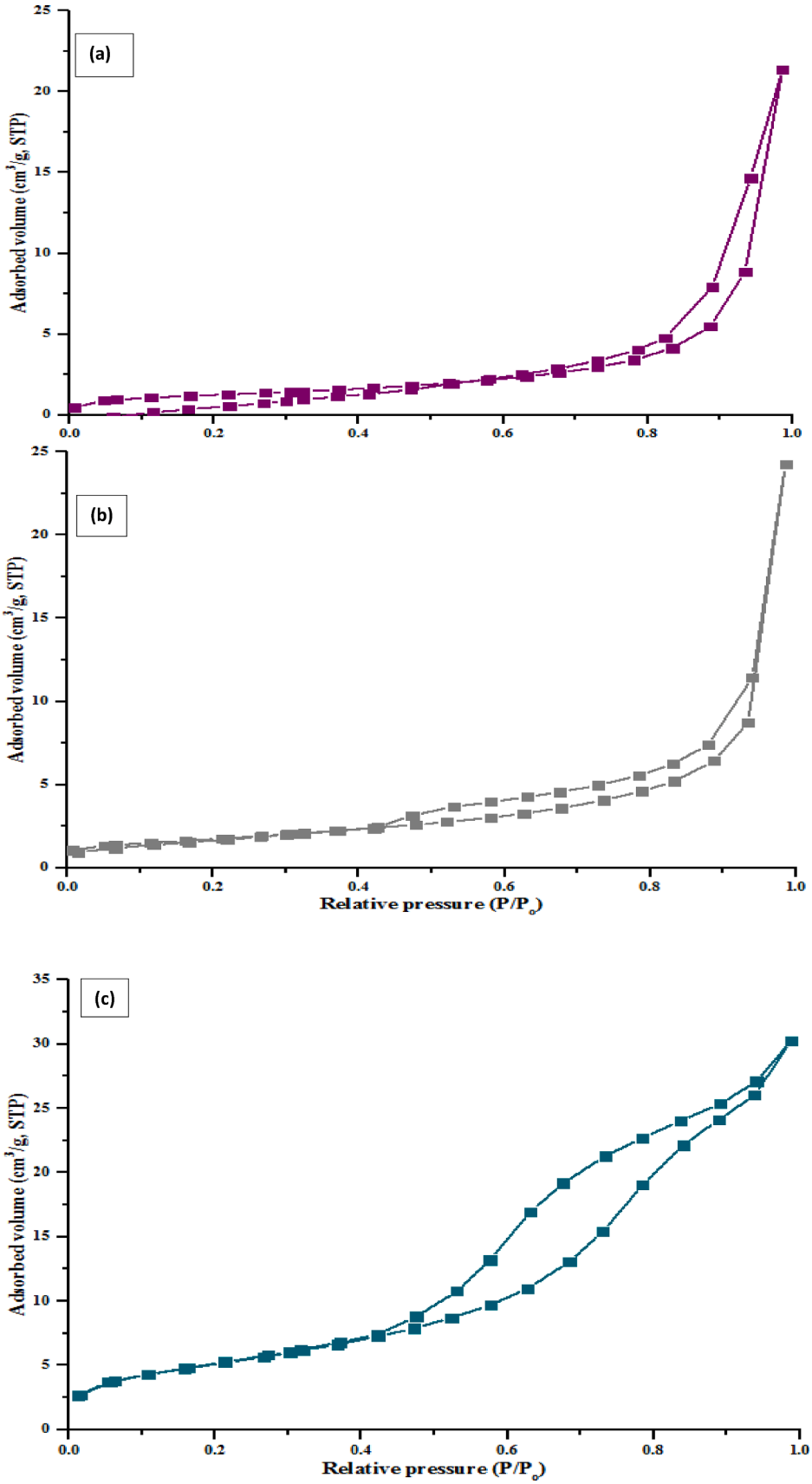

Fig. 5. N_2 adsorption/desorption isotherms for (a) Na-TiO_2 (b) N/Fe-TiO_2 (c) N/Na/Fe-TiO_2.

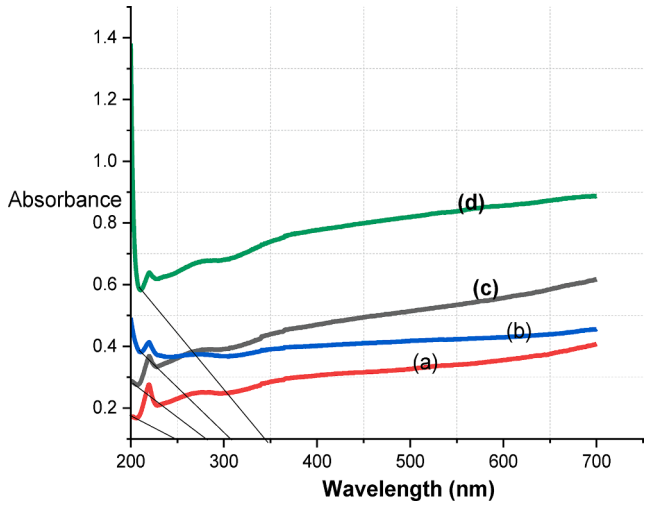

Fig. 6. UV spectra of (a) Na-TiO_2 (b) N/Fe-TiO_2 (c) Pure TiO_2 (d) N/Na/Fe-TiO_2.

ionized water was added to dilute the extract, and 5 cm^3 of 0.1 M titanium (IV) isopropoxide (TTIP) was added dropwise over 2 h on a magnetic stirrer (SCILOGEX ms-H280-Pro) at 2000 rpm. To adjust the pH of the solution to the desired pH 3, 0.5 M HCl was added in drops, followed by the formation of white precipitates of hydrous titanium hydroxide. After 2 h of stirring, the precipitates were collected by centrifugation for 15 min at 5000 rpm (Universal Centrifuge-PLC-012E). To remove unreacted ions, the nanoparticles were washed several times with 70 % ethanol and then with de-ionized water. The separated nanoparticles were oven-dried for 2 h at 80 °C before being calcined in a muffle furnace (Surgifriend medicals Sm9080) at 550 °C for 2 h.

Modification of TiO_2 nanoparticles with nitrogen, sodium, and iron

The nitrogen, sodium, and iron tri-doped TiO_2 nanoparticles were prepared using the method described by El Nemr et al. [13]. In this case, 50 cm^3 of the prepared bitter leaf extract was measured into a 250 cm^3 beaker, followed by adding 5 cm^3 of titanium(IV) isopropoxide dropwise with vigorous stirring for 20 min to prepare solution A. Then, 100 cm^3 of de-ionized water, known weight of $NaNO_3$, NH_4NO_3, and $FeCl_3{\cdot}6H_2O$ were mixed to make solution B. The dissolved amounts correspond to molar ratios of N, Na, and Fe of 1 %. After 40 min of vigorous stirring, solution A was added dropwise to solution B, stirring at 200 rpm for 2 h. After centrifugation, the precipitates were washed copiously with de-ionized water, oven-dried at 80 °C overnight, and then calcined at 550 °C for 2 h.

Characterization of TiO_2-based photocatalysts

The as-prepared catalyst phase structure and crystallite size were determined using a powder X-ray diffraction (XRD) model Bruker AXS D8 with CuK radiation, which was operated under the following conditions: 40 kV applied voltage, 40 mA current, and 0.05°/s scanning rate. The XRD patterns were taken over a 2 theta = 20° to 90° range. The particle size distributions were determined using a high-resolution transmission electron microscopy (HRTEM) (Zeiss Auriga model, USA). The orbital type, binding energy, and oxidation state of the prepared nanomaterials were determined using an X-ray photoelectron spectrometer (XPS), XPS PHI 5400 outfitted with a hemispherical sector analyzer and operated with non-monochromated Al K X-rays with an energy of 1486.6 eV at 300 W and 15 kV. The surface areas of the synthesized samples were investigated using the Brunauer-Emmett-Teller (BET) model NOVA2400e. A Shimadzu UV–visible spectrophotometer 1800 was used to determine the optical absorption properties of the photocatalysts. The reference material is $BaSO_4$. The optical

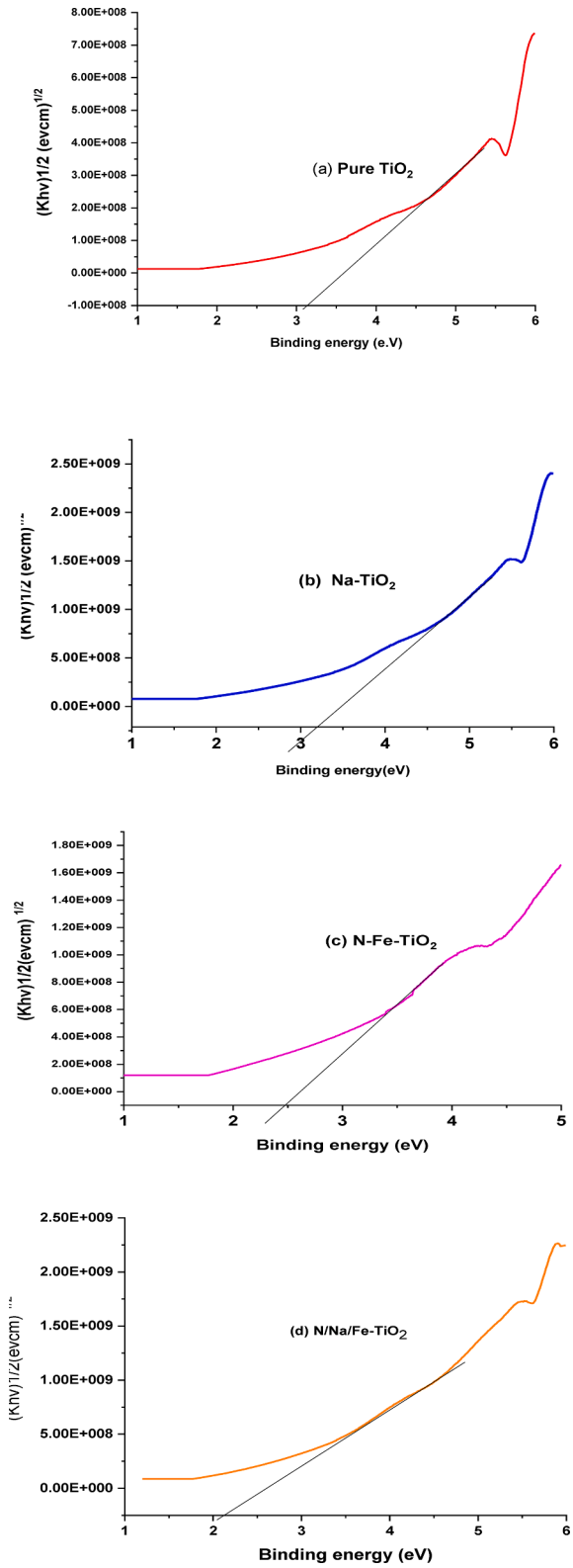

Fig. 7. Band gap energy (Tauc) Plot of $(ahv)^{1/2}$ versus *hv* of (a) pure TiO_2 (b) Na-TiO_2 (c) N/Fe-TiO_2 (d) *N*-Na-Fe-TiO_2.

properties of the catalysts were studied using photoluminescence (PL) (Perkin Elmer LS 55), the excitation wavelength of 320 nm. A Fourier transform infrared spectrophotometer was used to determine the chemical composition (FTIR, Thermo Fisher Scientific Nicolet iS5, USA).

Table 3
The energy bandgap of pure and doped TiO_2.

Samples	λ(nm)	Bandgap energy (nm)
Pure TiO_2	275	3.12
Na- TiO_2	242	3.09
N/Na- TiO_2	278	2.32
N/Na/Fe- TiO_2	312	2.10

Photocatalytic degradation experiments

The photolysis experiment was initially carried out without synthetic photocatalysts to see how visible light affected MG. A 300 W tungsten halogen lamp was used as a visible light source, with the wavelength of visible light varying from 380 nm to 750 nm. A 100 ppm MG solution was irradiated under visible light for 2 h. Before starting the photocatalytic degradation reaction, adsorption studies were performed in the dark on all of the produced photocatalysts to evaluate the degree of adsorption and the duration required for adsorption equilibrium. 50 cm^3 of MG solution (50 ppm) was added to 0.1 g photocatalyst in a beaker

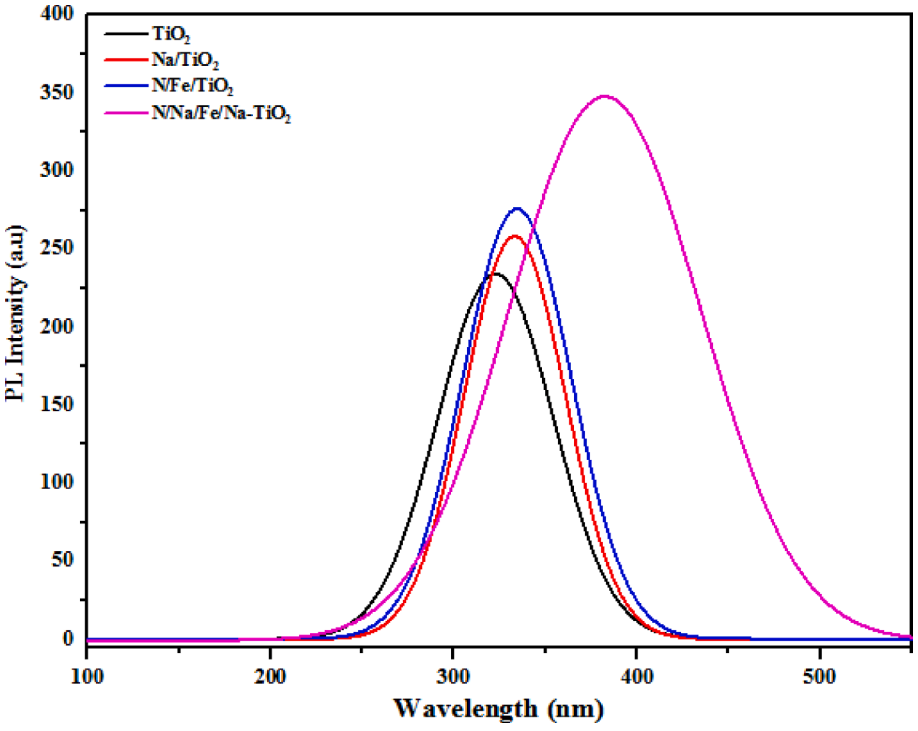

Fig. 8. Photoluminescence spectra of TiO_2, Na/TiO_2, $N/Fe/TiO_2$, and $N/Na/Fe/Na\text{-}TiO_2$ with the excitation wavelength of 320 nm.

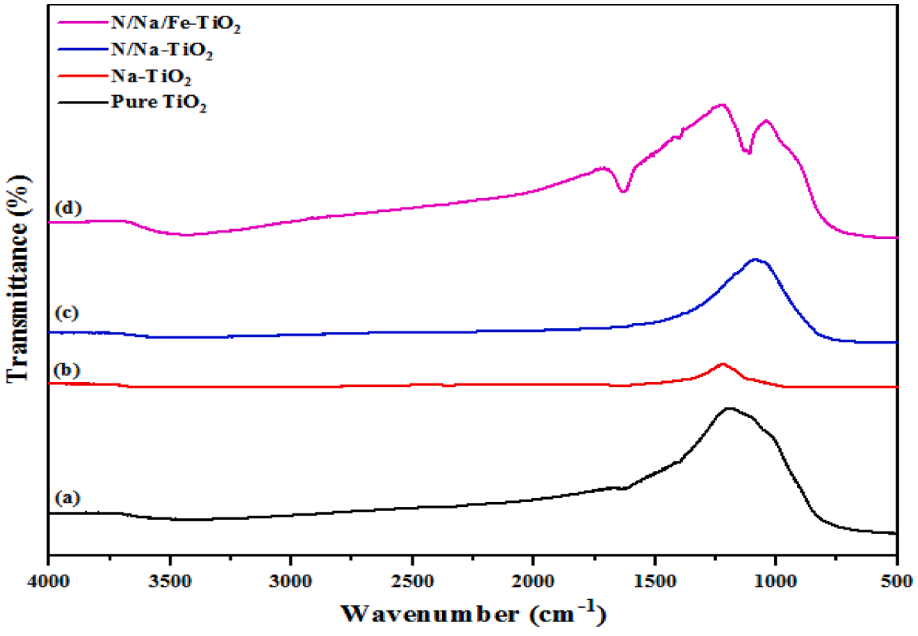

Fig. 9. FTIR spectra of (a) pure TiO_2 (b) $Na\text{-}TiO_2$ (c) $N/Fe\text{-}TiO_2$ (d) $N/Na/Fe\text{-}TiO_2$.

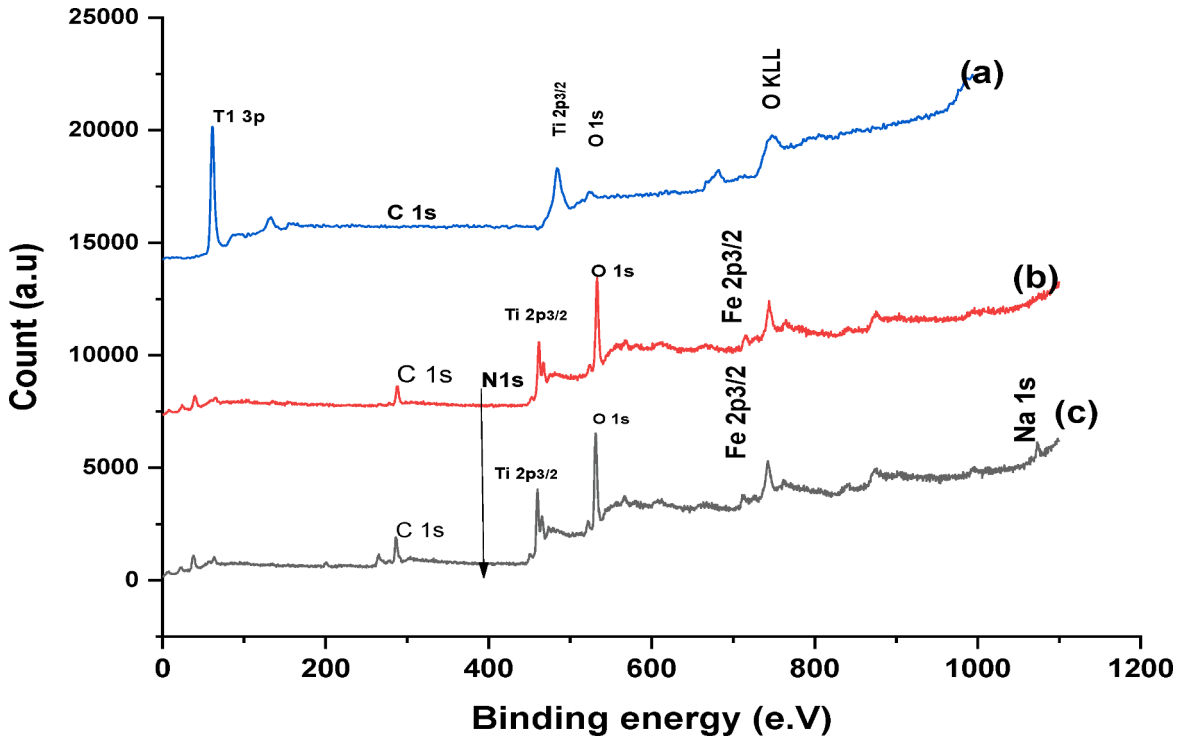

Fig. 10. XPS survey spectra of (a) bare TiO_2 sample (b) N/Fe-TiO_2 (c) N/Na/Fe-TiO_2.

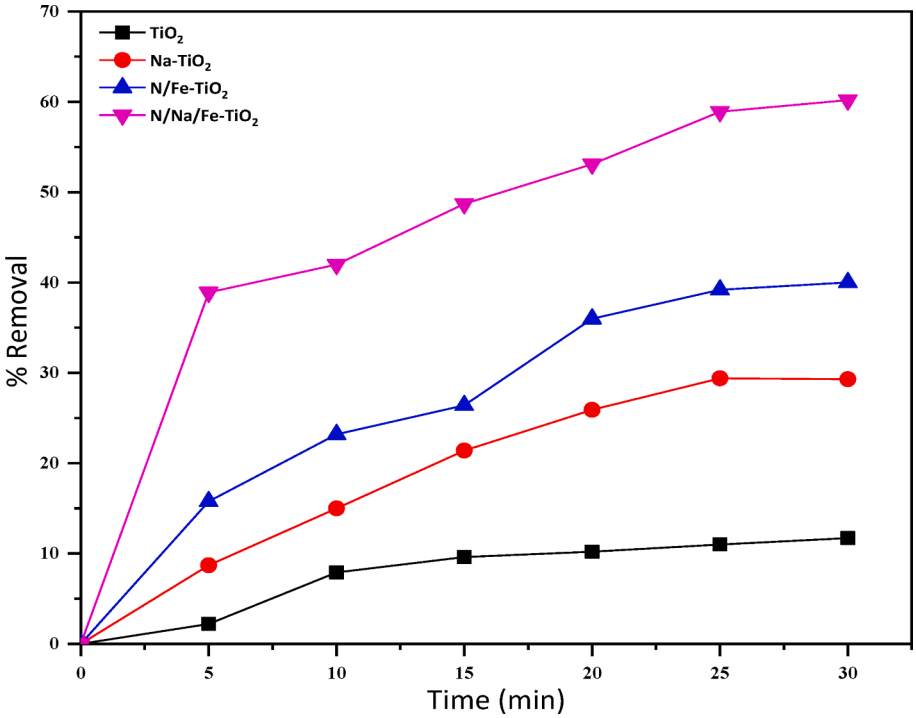

Fig. 11. Adsorption activities of bare TiO_2, Na-TiO_2, Na/Fe-TiO_2, and N/Na/Fe-TiO_2 for degradation of MG dye in the dark (absence of visible light radiation).

and stirred in the dark for 1 h. TiO_2 nanocatalyst attained adsorption–desorption equilibrium within 30 min for MG removal. The photocatalytic experiments were carried out in a home-built photoreactor at ambient temperature and pressure. In a typical run, the photocatalytic potential of different photocatalysts was investigated at 50 ppm of malachite green. A known mass of 0.1 g of the prepared photocatalysts was suspended in 50 cm^3 of MG dye solution and then stirred for 30 min in the dark to attain adsorption–desorption equilibrium. Afterward, the suspension was irradiated under continuous stirring for 1 h, and samples were withdrawn at regular intervals. The mixtures were filtered using 0.22 μm filter paper, and then the filtrates were analyzed to monitor the change in dye concentrations. The MG dye concentration was determined at $\lambda^{max} = 420$ nm by a UV–visible spectrophotometer. The initial absorbance of the MG dye solution was determined before the

Table 4
Kinetic parameters for the adsorption of MG dye on bare TiO_2 and modified TiO_2 nanoparticles.

Samples	First-order			Second-order		
	$k_1((min^{-1})$	$q_{e(mg/g)}$	R^2	k_2(g/mg.min)	q_e(mg/g)	R^2
Na-TiO_2	0.1033	12.547	0.5894	0.1150	20.534	0.9566
N/Fe-TiO_2	0.1048	13.326	0.5713	0.0083	22.523	0.9143
N/Na/Fe-TiO_2	0.0289	3.458	0.0504	0.145	24.231	0.9879
TiO_2	0.0664	7.327	0.4607	0.0458	17.153	0.9806

experiment, and the final absorbance value of MG dye in the filtrate was also determined. The percentage degradation obtained for each photocatalyst was calculated according to Equ. (1).

$$\text{Degradation}\ (\%) = \frac{C_o - C}{C_o} \times 100 \quad (1)$$

where C_o is the initial dye absorbance before photocatalytic/adsorption, and C is the absorbance at any time t, during degradation.

Design of experiment

In this study, the Box Behnken Design (BBD), a popular type of RSM, was used to optimize the photocatalytic degradation process. Three independent variables were chosen to investigate the effect of operating parameters on the photocatalytic degradation efficiency of textile dye: irradiation reaction time (min), catalyst dosage (g), and dye solution pH. After completing seventeen experimental runs, the data was examined using the design expert software version 11.0.0. Table 1 depicts the experimental ranges of independent dye removal and amounts.

Photocatalyst reusability studies

This study examined the reusability of the best-suited catalyst to assure its long-term stability. The N/Na/Fe tri-TiO_2 photocatalyst was filtered, rinsed with de-ionized water, and recalcined at 550 °C for 2 h

Table 5
Kinetics data for the photocatalytic degradation of MG dye.

Samples	First-order			Second-order		
	$k_1((min^{-1})$	$q_{e(mg/g)}$	R^2	k_2(g/mg.min)	q_e(mg/g)	R^2
Fe-TiO_2	0.110	39.762	0.8715	0.000456	31.813	0.1680
Na-TiO_2	0.0983	23.388	0.9220	0.00121	22.362	0.3924
N/Na/Fe-TiO_2	0.113	34.765	0.9625	0.00132	28.314	0.4628
TiO_2	0.0802	20.836	0.8438	0.000126	11.728	0.0209

Table 6
The predicted and actual results of MG dye degradation over (2:1:1) N/Na/Fe-TiO_2 nanocatalyst photocatalyst.

Experimental run	Independent variables			(% Degradation of MG)	
	A: Contact Time (min)	B: Dosage (g)	C: Solution pH	Actual removal	Predicted removal
1	5	0.15	3	35.00	33.12
2	30	0.15	3	45.00	45.62
3	17.5	0.15	6.5	70.00	72.00
4	17.5	0.15	6.5	70.00	72.00
5	17.5	0.1	10	90.00	88.75
6	5	0.2	6.5	55.00	55.62
7	30	0.1	6.5	80.00	79.37
8	17.5	0.15	6.5	75.00	72.00
9	17.5	0.15	6.5	75.00	72.00
10	30	0.15	10	95.00	96.87
11	17.5	0.2	3	50.00	51.25
12	17.5	0.1	3	40.00	40.00
13	5	0.15	10	60.00	59.37
14	5	0.1	6.5	50.00	51.87
15	17.5	0.15	6.5	70.00	72.00
16	30	0.2	6.5	80.00	78.12
17	17.5	0.2	10	80.00	80.00

Key: A = Contact time, B = Catalyst dosage, C = pH.

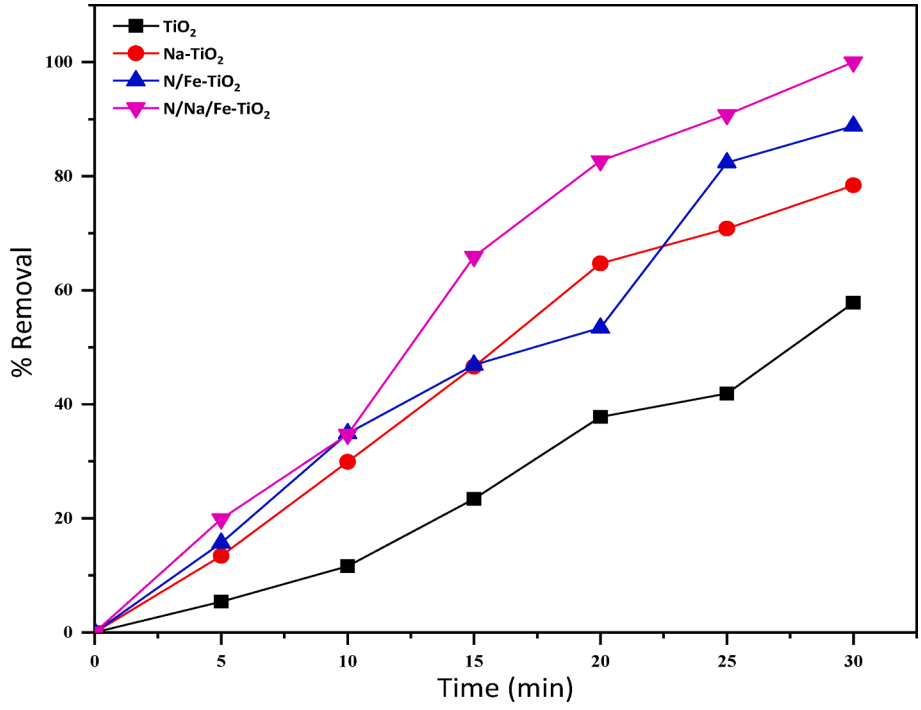

Fig. 12. Photocatalytic activities of bare TiO_2, Na-TiO_2, Na/Fe-TiO_2, and N/Na/Fe-TiO_2 in the degradation of MG dye under visible light radiation.

Table 7
ANOVA of the quadratic model for photodegradation of MG dye.

Source	Coefficient estimate	F-value	p-value	
Model		78.38	< 0.0001	significant
A-Reaction Time	12.50	179.49	< 0.0001	significant
B-Catalyst Dosage	0.6250	0.4487	0.5244	Not significant
C-Solution pH	19.38	431.22	< 0.0001	significant
AB	−1.25	0.8974	0.3750	Not significant
AC	6.25	22.44	0.0021	Significant
BC	−5.00	14.36	0.0068	Significant
A^2	−6.00	21.77	0.0023	Significant
B^2	0.2500	0.0378	0.8514	Not significant
C^2	−7.25	31.78	0.0008	Significant
Lack of Fit		0.8333	0.5413	Not Significant

Key: DF = degree of freedom of different source, F-value = Fisher value; degree of freedom, P = probability; $R^2 = 0.9902$, Adjusted $R^2 = 0.9775$ and Predicted $R^2 = 0.9301$.

after each reaction. The photocatalytic experiment was repeated following the same conditions using the re-used catalysts for five consecutive cycles.

Results and discussion

Characterization

XRD analysis

The crystal structure and phase of the synthesized pure TiO_2 and multiple doped TiO_2 samples were investigated using XRD, and the corresponding XRD pattern is presented in Fig. 1.

As shown in Fig. 1, strong, sharp, intense, and well-defined diffraction peaks were observed for bare TiO_2, Na-TiO_2, and N/Na/Fe-TiO_2 doped TiO_2 nanoparticles at 2theta values of 25.3°, 37.8°, 48.0°, 55.1°, 62.6°, 68.8°, and 75.7° corresponding to crystal planes (101), (004), (200), (211), (204), and (215) (JCPDS files No-00 021 1272). The result agreed with the finding of Mustapha et al. [33,34] for a typical anatase phase of TiO_2 nanoparticles irrespective of the dopants. Diffraction peaks at 27.4° and 36.0°, corresponding to (110) and (101) crystal planes (JCPDS No. 21-1276), corresponding to rutile observed in N/Fe-TiO_2 and absence in other samples showed that nitrogen and sodium-doping could successfully prevent the presence of TiO_2 rutile phase. There were no significant changes in the 2 θ position (101) diffraction peaks of all as-prepared samples, as shown in Fig. 1. This could be due to the low percentage of dopants, as the intensity of the (101) was slightly increased with the addition of N/Na/Fe, signifying a decrease in crystallite size compared to single-doped TiO_2. When the ionic radius of nitrogen (0.65), sodium (1.80), and iron (1.40) is compared to that of oxygen (0.60) and titanium (1.40), the relatively large variation in crystallite size indicates a significant change in the crystal structure in doped TiO_2 samples. In contrast, the most intense anatase (101) peak becomes slightly wider with the incorporation of N, Na, and Fe, indicating the intense peak intensity and the decrease in crystallite size compared to single-doped. The width of the (101) peak of the TiO_2 anatase phase was used to calculate crystallite sizes using Scherrer's Debye-equation. The particle size was observed to be 10–15 nm for pure TiO_2 and 5–7 nm for N/Na/Fe tri-doped samples, indicating that N, Na, and Fe dopants were introduced into the TiO_2 lattice but had no effect on the crystallization process.

HRTEM analyses

Figs. 2, 3, and 4 present the typical HRTEM images of the prepared pure TiO_2, N/Fe-TiO_2, N/Na/Fe-TiO_2 nanocatalysts annealed at 550 °C. Undoped TiO_2 and N/Fe-TiO_2 exhibited well aggregated and homogeneously distributed spherical shape nanoparticles with average particle sizes of 6–10 nm and 11–16 nm, respectively, which correspond to the size obtained from XRD measurements. The SAED images show the polycrystals class of TiO_2, which agrees with the biphasic anatase and rutile structure obtained from the X-ray diffractograms. More intriguingly, the SAED pattern of pure TiO_2 and N/Na/Fe-TiO_2 clearly shows a well-defined concentric ring caused by diffraction from the anatase and rutile TiO_2 planes (101), (004), (200), and (211). However, the bright spot became clearer in N/Na/Fe-TiO_2 sample, an indication of relatively higher crystallinity in comparison to sample N/Fe-TiO_2.

Surface area measurement

Table 2 shows the results of the BET surface area, pore volume, and pore size of the synthesized pure TiO_2 and doped TIO_2. At a relative pressure range of 0.4–0.9, all doped TiO_2 nanocatalysts display H2 hysteresis loop characteristics, corresponding to type IV adsorption isotherm, indicating that all doped samples have a better surface area, mean pore diameter, and pore-volume than un-doped samples. The surface area (80.16 m^2/g) and pore size (5.29 nm) of sample N/Na-Fe-TiO_2 were the greatest in the BET analysis. The hysteresis curve (type 4 adsorption isotherms) reveals ink bottle-like holes in the material (Fig. 5c). The BET surface area rises in the following order: bare TiO_2 < Na-TiO_2 < N/Fe-TiO_2 < N/Na/Fe-TiO_2. The materials were mesoporous, as shown by the average pore size in Table 2. Furthermore, compared to pure TiO_2, the pore volume of Na-TiO_2, N/Fe co-doped TiO_2, and N/Na/Fe-tri-doped TiO_2 is slightly reduced. The presence of a dopant slows the growth of TiO_2 nanoparticles, according to this finding.

UV analysis

Figs. 6 and 7 show the UV spectra and bandgap energy plots of bare TiO_2, Na-TiO_2, N/Fe-TiO_2, and N/Na/Fe-TiO_2 nanocatalysts, respectively. Doping TiO_2 nanoparticles with N, N/Na, or N/Na/Fe resulted in a significant redshift in the absorption threshold value to longer wavelengths and visible light. Tauc's equation which describes a link between the absorption coefficient and the incident photon energy of semiconductors as presented in Equ. 2, was used to calculate the optical bandgap from the absorption data of each sample.

$$khvn = B(hvE_g) \quad (2)$$

where B is a constant, n is the indirect bandgap exponent of 2, and Eg is the optical bandgap. Table 3 shows the energy bandgap (Eg) of the generated samples. Plotting $(khv)^{1/2}$ vs h and extrapolating the linear component of the absorption edge is presented in Fig. 7.

When TiO_2 is tri-doped using N, Na, and Fe, the improvement in absorption characteristics is more pronounced, as presented in Table 3. These findings demonstrate that tri-doping TiO_2 with N, Na, and Fe is more successful than co-doping with N, Na, or N, Fe. This behaviour could be explained by Fe, Na, and N having a stronger cation–anion cooperative action than Na, N, or N, Fe alone. The cation–anion suitable effect influences the bandgap value, which has a substantial mutual structural influence. The increase in UV–vis absorbance raises the photogenerated electrons and holes available to contribute to the photocatalytic activity of TiO_2.

PL analysis

The photogenerated charge carrier separation and recombination in TiO_2 and nanocomposites were measured using photoluminescence. The PL spectra described in Fig. 8 were recorded for TiO_2, Na/TiO_2, N/Fe/TiO_2, and N/N/Fe/Na-TiO_2, which the peaks appeared at 324, 333.72, 336.29, and 383.48 nm, respectively. The PL peak shape and position of photocatalysts are non-identical under the same excitation wavelength,

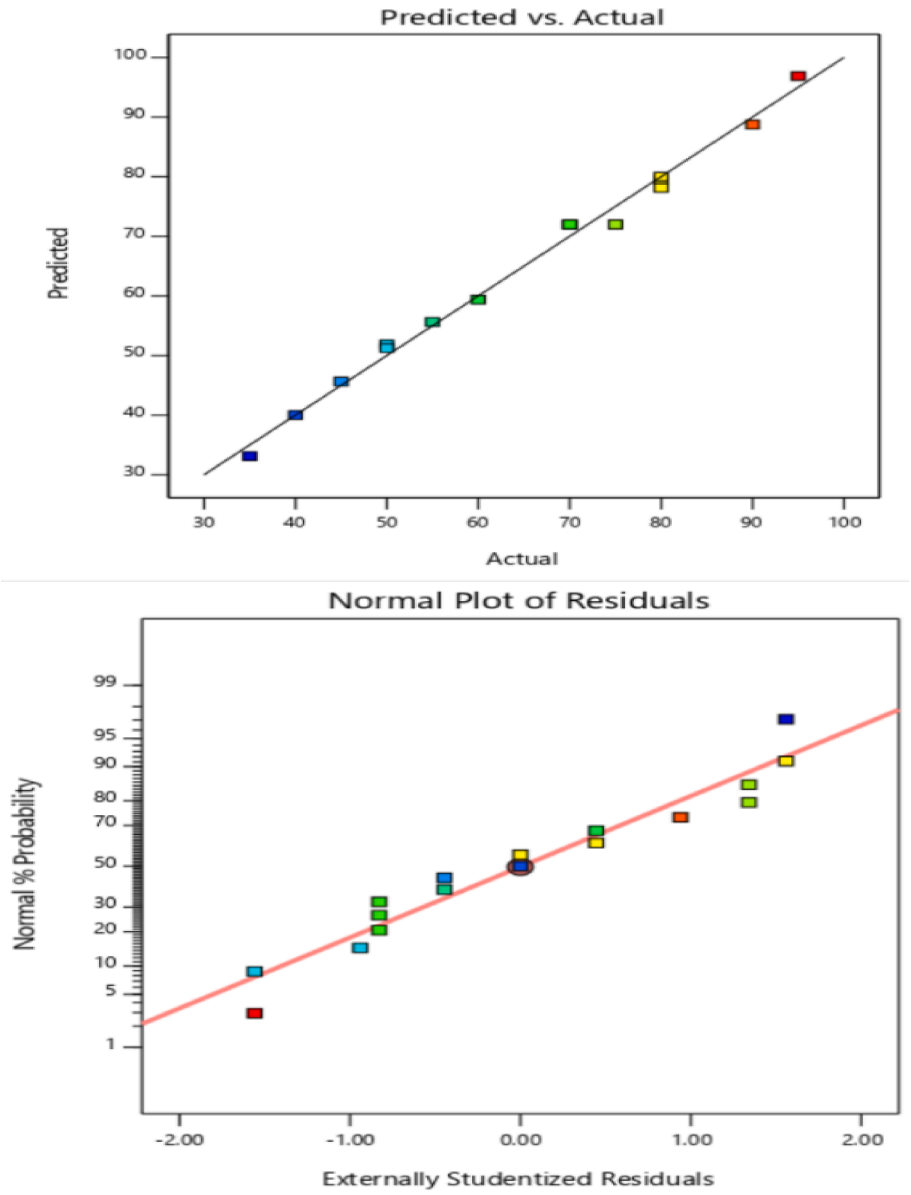

Fig. 13. (a) Plot of predicted versus experimentally observed values in the degradation of malachite green dye catalyst (b) Normal plot of residuals.

indicating that the PL mechanism is not the same. A broad PL band of N/Na/Fe/Na-TiO_2 could be ascribed to overall exciton emission due to trapping free exciton by titanate groups near defects. This is similar to the finding of Xie et al. [51], who reported that a strong peak found for Se-doped TiO_2 but lacking in TiO_2 was due to high defects concentration leading to significant suppression of electron-hole recombination in TiO_2. The N/Na/Fe/Na-TiO_2 exhibits significant photocurrent and increased charge carriers. It was observed that the excitonic absorption maxima moved toward the blue region with an increasing doping system. As TiO_2 was doped, energy levels were established between the conduction and valence band. Doping increases the bands of the nanocomposites. In this study, PL emissions of the nanocomposites show a blue-shifted emission. This contradicted a survey by Mannaa et al. [28], who concluded that adding Ni^{2+} ions to TiO_2 decreased PL intensities and a significant red shift of emission PL peaks.

FTIR analysis

Fig. 9(a) represents bare TiO_2. Peaks centred at 1638 cm^{-1} and 3450 cm^{-1} indicate surface-adsorbed water and hydroxyl groups in these spectra [2,34]. The C—H stretching band had no peak at 2900 cm^{-1} in Fig. 9(a, b, and c), indicating that all organic chemicals were removed from the samples as a consequence of calculations. The band at 1638 cm^{-1} found in the Na-TiO_2 spectrum was attributed to the bending vibrations of the O—H bond, as seen in Fig. 9(b). The presence of additional hydroxyl groups on the titania surface supported the enhancement of photocatalytic activity [17]. Furthermore, the band at 1216 cm^{-1} can be attributed to ambient CO_2 adsorbed stretching vibrations and stretching and bending vibrations for moisture [20].

Fe-N-TiO_2 showed additional peaks at 1047 cm^{-1} compared to Na-TiO_2 and bare TiO_2, which can be attributed to the vibration of the N–Ti link created when N atoms are incorporated in the TiO_2 network (Feng et al., 2019). Fe-O-Ti was not detected at 570 cm^{-1}, possibly due to its low iron doping level. Fig. 9(d) shows the FT-IR spectra of N, Na, Fe tri-doped TiO_2. As displayed in Fig. 9(c), the spectra show the shift in Ti-O-Ti characteristics peak to the higher wavelength at 493.50 cm^{-1} [20]. Interestingly, a shift of the Ti-O-Ti band observed for bare TiO_2 shifted to a lower wavenumber as observed for N, Na, and Fe tri-doped samples. This observation indicates the existence of structural defects. This is in agreement with the XRD results, which indicate the band shift due to the formation of Fe-O, Na-O, and N—O bonds during the substitution of Ti^{4+}

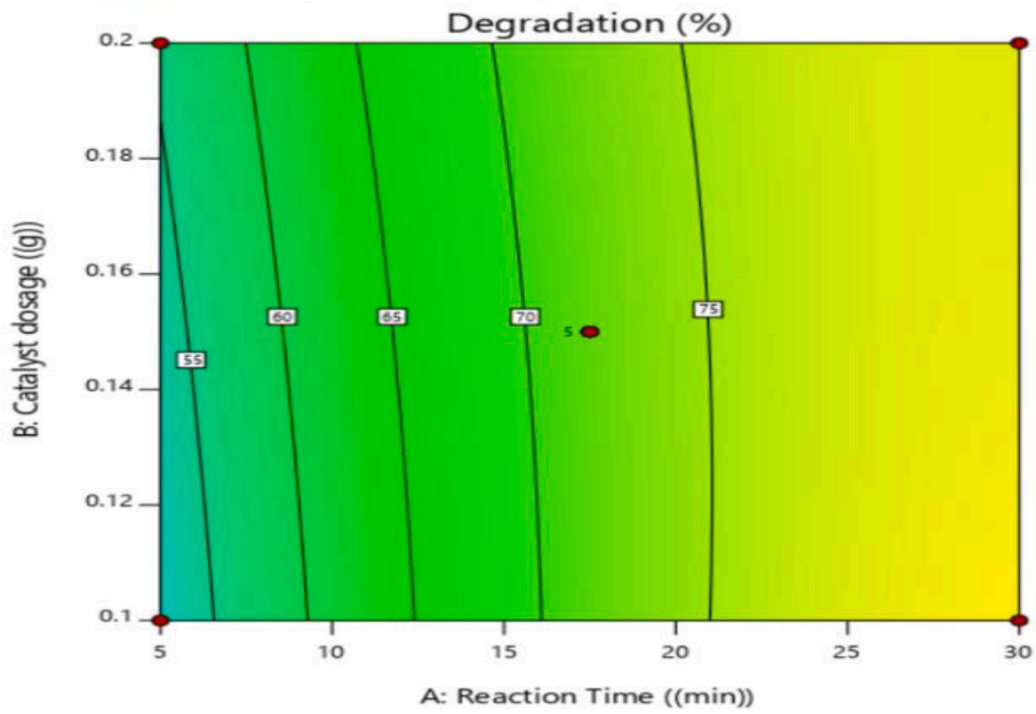

(a)

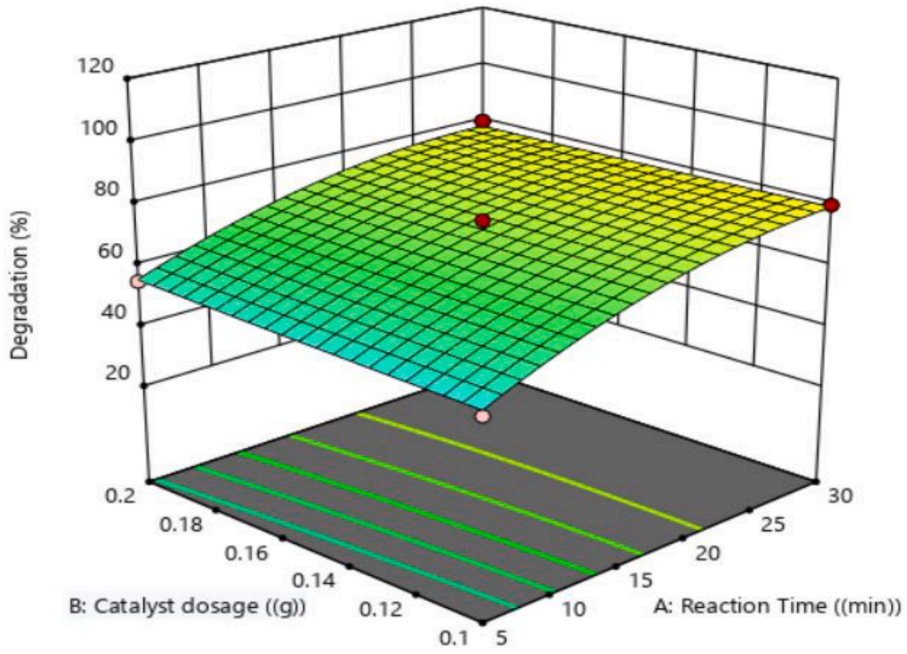

(b)

Fig. 14. (a) 3D Response surface interaction between reaction time and catalyst dosage at a constant pH of 6.5 for visible-light-induced Photocatalytic decolourization of MG dye (b) contour plot.

with Fe^{3+} and Na^{+}, and Ti^{4+} with nitrogen ion within the TiO_2 framework. Also, N—H on the peaks of 3150–3600 cm^{-1} was observed for N/Na/Fe-TiO_2 samples [18]. In addition, the peak appearing at 1142.95 cm^{-1} was attributed to the C—C vibration of the C-C skeleton [23], while peaks detected at 1651.84 cm^{-1} are ascribed to the stretching vibration of the H—O—H bond from the surface-adsorbed H_2O, OH, or COOH groups [31].

XPS analysis

XPS tool was used to determine the composition and chemical states of the nanocatalysts as they were manufactured. The XPS survey spectra of the catalysts are shown in Fig. 10.

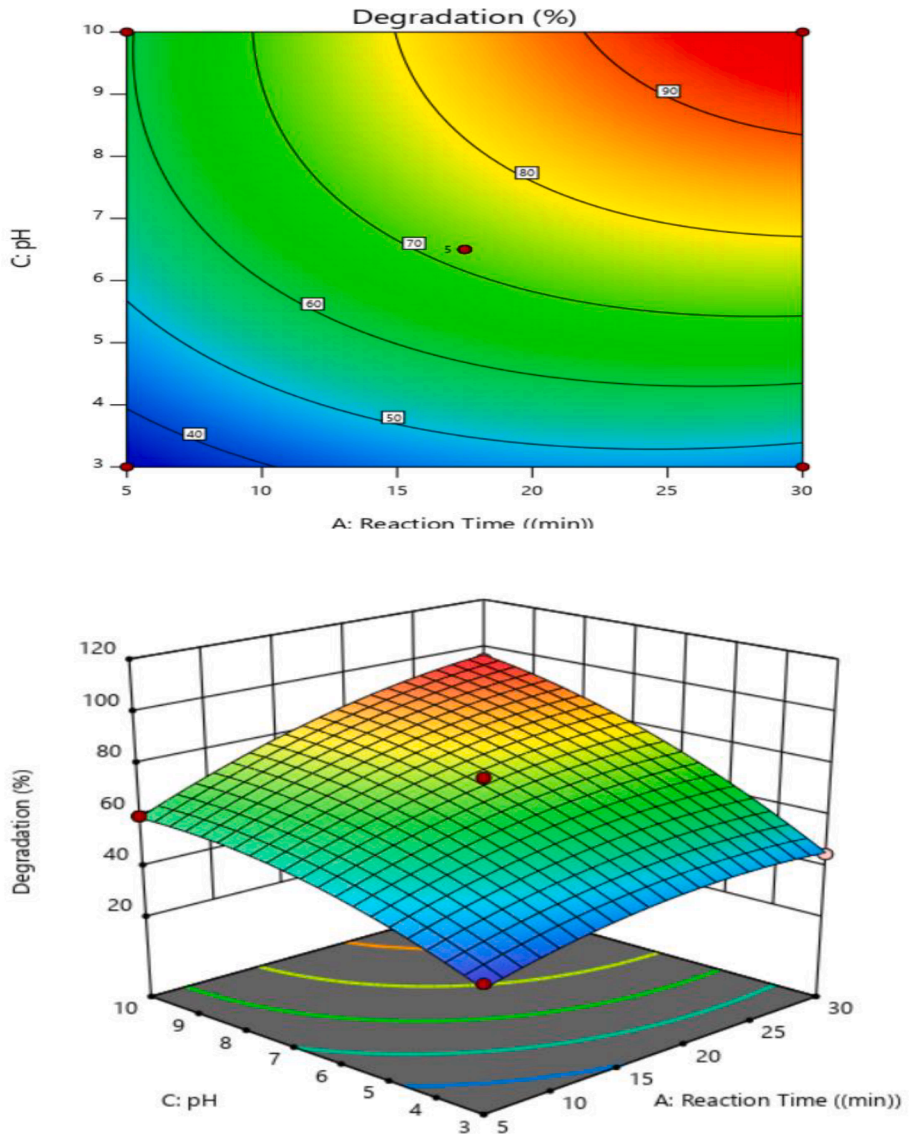

Fig. 15. (a) 3D Response surface interaction between reaction time and solution pH at a constant catalyst dosage of 0.15 g for visible-light-induced Photocatalytic decolourization of malachite green (b) Contour plot.

The signal peaks at 458.76 eV, 466.2 eV, 531.71, and 286.50 eV are associated with the binding energy of $Ti2p_{1/2}$, $Ti2p_{3/2}$, O 1 s, N 1 s, Fe 2p, and C 1 s, respectively. The C 1 s peak was present in all prepared samples, a signal that originated from the plant extract adopted for the green synthesis process. No other impurity peaks were observed, which proves the bare TiO_2 sample contains only three elements (Ti, O, and C). The XPS spectra of Ti 2p in Fe/N-TiO_2 and N-Na-Fe-TiO_2, as presented in Fig. 10(b and c), reveal that the Ti $2p_{3/2}$ and Ti $2p_{1/2}$ peaks at 461.36 eV; 467.24 eV (N/Fe-TiO_2) and 459.36 eV; 465.33 eV (N-Na-Fe-TiO_2), respectively were in a favourable agreement with those previously observed for Ti^{4+} [56,10]. Obviously, a reduction in titanium binding energy upon simultaneous doping TiO_2 with N, Na, and Fe observed in Fig. 10(b and c) could be attributed to the formation of O-Ti-Na, Ti-O-Fe, and Ti—O—N in the TiO_2 lattice [10]. The presence of N in N/Fe-TiO_2 and N-Na-Fe- TiO_2 nanoparticles were validated by the N 1 s spectra and significant peaks around 400 eV, which corroborated the formation of anionic N in O–Ti–N linkage [24]. The peak at 1072.67 eV corresponds to Na 1 s, showing the presence of Na in the lattice of the N-Na-Fe-TiO_2. It was evident that the O 1 s binding energies of N-Na-Fe-TiO_2 are strongly shifted to lower binding energies at 530.60 eV compared with the bare TiO_2 (531.70 eV). This observation is attributed to surface hydroxyl oxygen groups formed by oxygen vacancies [43]. This indicates that the N/Na/Fe-TiO_2 has more hydroxyl groups on its surface than N-Fe-TiO_2 and bare TiO_2, thus enhancing the hydrophilicity of N-Na-Fe-TiO_2.

Also, the Fe $2p_{3/2}$ peaks observed at 718.30 eV and 712.08 eV for N/Fe-TiO_2 and N-Na-Fe-TiO_2 nanocatalyst, respectively, indicate the existence of Fe in +3 oxidation state [36,39]. The Fe^{3+} with an ionic radius of 0.064 nm penetrates the TiO_2 structure (ionic radius is 0.068 nm) for a six-coordinated number. The Fe ions may lead to the formation of the Ti-O-Fe bond, indicating the successful incorporation of Fe(III) onto the TiO_2 lattices. The formation of Ti-O-Fe would change the electron density as a result of its role as h^+/e^- traps resulting in different electronegativity. The observation in this study corresponds to the XPS result of Fe-N co-doped TiO_2 photocatalysts reports by Zhao et al. [58].

Adsorption studies

Adsorption behaviour of MG dye using prepared nanocatalysts (Na-TiO_2, N/Fe-TiO_2, and N/Na/Fe-TiO_2) in the dark was performed as control experiments and presented in Fig. 11. Overall, the removal efficiency of malachite green dye was 11.7 %, 29.3 %, 40.01 %, and 60.2

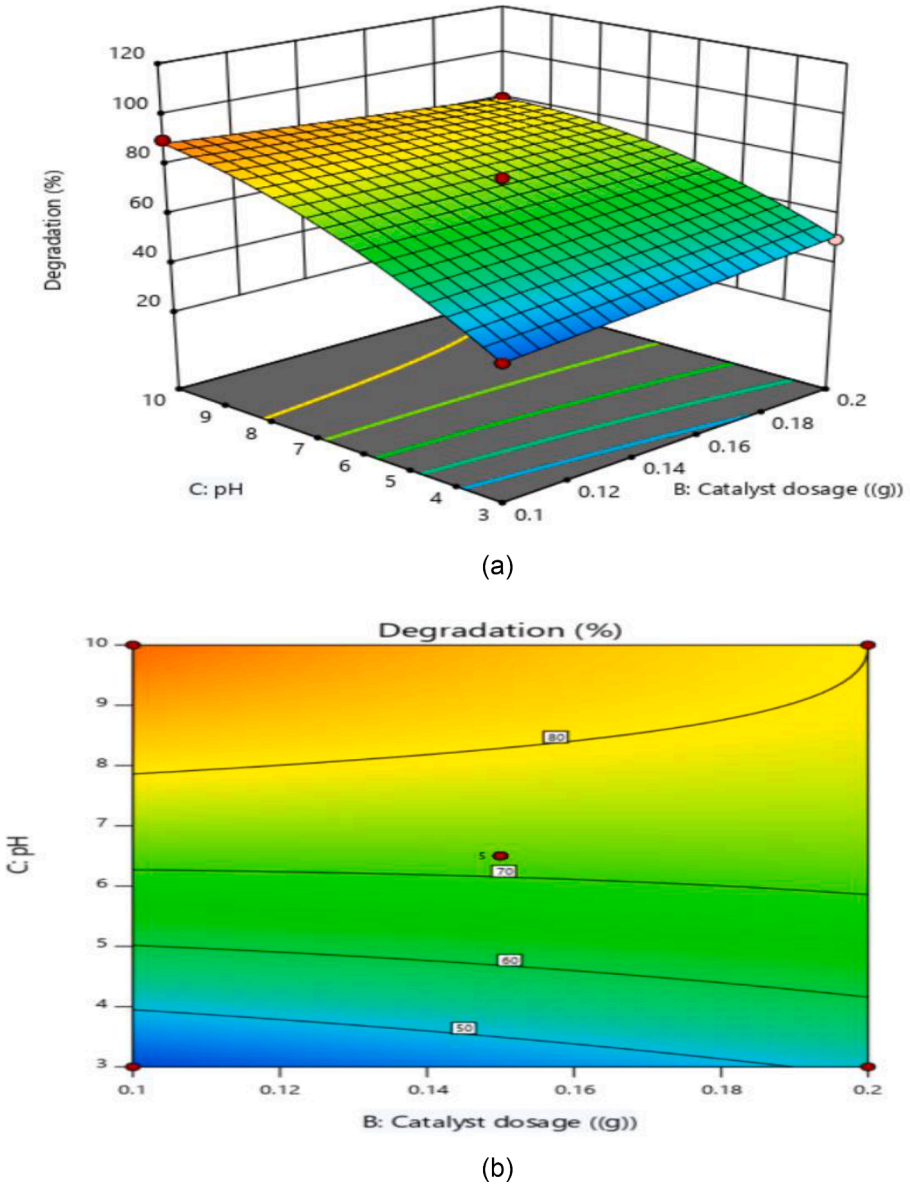

Fig. 16. (a) 3D Response surface interaction between catalyst dosage and solution pH at a constant reaction time of 17.5 min for Visible light-induced Photocatalytic decolourization of MG dye. (b) contour plot.

% for pure TiO_2, Na-TiO_2, N/Fe-TiO_2, and N/Na/Fe-TiO_2, respectively. The adsorptive potentials of MG by all photocatalysts were moderate in order of; N/Na/Fe-TiO_2 > N/Fe-TiO_2 > Na-TiO_2 > Bare TiO_2. The pseudo-first-order and pseudo-second-order kinetic models were adopted for the kinetic studies. Based on the results obtained from the linear plot between log qe-qt versus t, the k_1, k_2, q_e, and R^2 values from the models were calculated from the slope and intercepted the graph and presented in Table 4. The obtained R^2 values for the pseudo-first-order are 0.5894, 0.5713, 0.0504 and 0.4607 for Na-TiO_2, N/Fe-TiO_2, N/Na/Fe-TiO_2 and TiO_2, respectively. The R^2 values for the pseudo-second-order are higher for the nanoadsorbents with corresponding adsorption capacities, as presented in Table 4. Thus, the rate of adsorption of dye molecules is controlled by the chemisorption mechanism. It can be observed that the adsorption did not conform to the pseudo-first-order model. As a result, the pseudo-second-order was suggested to represent the adsorption of MG dyes by single-doped TiO_2, double-doped-TiO_2, and Tri-doped TiO_2 nanocatalysts. The dissimilarity in the rate constant and correlation coefficient exhibited by each catalyst is attributed to the difference in surface area, particle size, and bandgap energy [55].

Photocatalytic studies

Fig. 12 shows the results of the photodegradation of MG dye collected under visible light using different nanocatalysts. The elimination of malachite green high absorption at 618 nm was measured in photocatalytic degradation tests utilizing bare TiO_2 and modified TiO_2 nanoparticles for the degradation of MG for comparison. The photocatalytic activity of the undoped TiO_2 nanocatalyst is less than the doped TiO_2, which only eliminated 58.19 % of the MG at 30 min. This finding suggests that bare TiO_2 should be modified to improve photocatalytic removal. Mayoufi et al. [30] obtained similar results for the degradation of Congo red under visible light irradiation using W—N—S tri-doped TiO_2. After 30 min of irradiation, the MG in the N/Na/Fe-TiO_2 sample had completely degraded. This is due to the synergistic effects of N, Na, and Fe on doped TiO_2, which caused the absorption edge to extend into the visible light spectrum, lowering the bandgap energy and thereby lowering the bandgap energy (Table 5). The increased degrading

Table 8
Comparison between the present study and recently published studies.

Catalyst	Preparation method of catalyst	Pollutant (Dyes)	Light source and optimum conditions	% Degradation	Reference
Fe-TiO_2	Hydrothermal method	Reactive red 3 dye	UV light Reaction Time = 30 min; dopant concentration = 0.2 wt%;	94 % bandgap 2.60 eV	Rivera et al. [38]
NiO/TiO_2	hydrothermal	Reactive black 5	Natural sunlight dye concentration of 40 mg/l, initial pH value of 5, catalyst dosage 2 g/l, and contact time of 150 min	86.1 % Bandgap = 3.86 eV	Salehi et al. [41]
Fe/C/S-TiO_2		Congo red	Visible light Contact time = 180 min Catalyst dosage = 0.02 g; dye solution concentration = 20 ppm	87.9 Surface area = 74.3 m^2/g Bandgap = 2.00 eV	Anku et al. [4]
N—S co-doped $TiO_{2/5\%rGO}$	Facile single step hydrothermal method	Reactive Orange 16 Methylene blue	Visible light Contact time 2 hrs Dye concentration 3.12 × 10^{-5} M catalyst dosage: 50 mg	MB = 95 % Reactive orange = 96 % Band gap = 2.77 eV Surface area = 142 m^2/g	Appavu and Thiripuranthagan, [5]
Fe/N-TiO_2	sol–gel hydrothermal	Acid Orange 7 (AO7)	Visible light irradiation Dosage = 20 g/L pH = 3	> 90 % Surface area = 211 Bandgap = 2.74 eV	Cheng et al. [10]
Pd/Ag/N-TiO_2	Hydrothermal	Malachite green	Visible light Dye concentration 10^{-5} M Catalyst dosage = 0.05 g Reaction time = 1 hr	75 % Bandgap 1.76 eV	Chauhan et al. [9]
CN-TiO_2	Sol-gel hydrothermal method	Direct red 16	Visible light Irradiation time 90 min Dye concentration = 25 ppm pH = 4 catalyst dosage = 1.5 g/L	90.5 % Bandgap = 1.7 eV	Zangeneh et al. [55]
TiO_2	Commercial source Degussa P25	Methylene blue	UV lamp catalyst loading = 0.5 g/L, pH = 11 initial MB concentrations = 10 mg/L	95.1 %	Tichapondwa et al. [47]
Fe-N-TiO_2	Sol-gel	Acid Orange 7 (AO7)	Contact time=(60 min photocatalyst dosage = 3 g/L initial dye concentration = 10 mg L^{-1}	83 %	Mancuso et al. [27]
N-Fe-$Gd_{2.0}$ -TiO_2	Sol-gel method	Methylene blue	Visible light Dye concentration = 10 mg/L; catalyst dosage = 0.1 g; Bandgap = 2.62; surface area = 113.6	97.4 %	Li et al. [24]
N-TiO_2	Wet impregnation method	Methylene blue	Solar light Irradiation time = 60 min; pH = 5.5; dopant concentration = 20 mg/ L Surface area = NA	89.3 %	Turkten and Bekbolet, [49]
N/Na/Fe-TiO_2	**Hydrothermal-assisted Green Synthesis**	**Malachite Green**	**Visible Light** dopant dosage = 0.11 g, contact time = 25.38 min and pH of 9.89 bandgap = 2.10 surface area = 80.16	**97.89 %**	**Present Study**

activity was attributed to the reduced bandgap energy and increased surface area of the multiple doped TiO_2 nanoparticles [22].

Optimization of the photocatalytic removal process

RSM was used to optimize the photodegradation of malachite green dye, with three independent variables: contact duration (A), catalyst dosage (B), and solution pH (C). The analysis was carried out using statistical software (Design-Expert Version 11.0). Multiple regressions were used to fit the following second-order polynomial model given in the equation to the data from BBD.

$$Y = \beta_0 + \beta_1 A + \beta_2 B + \beta_3 C + \beta_{12} AB + \beta_{13} AC + \beta_{23} BC + \beta_{11} A^2 + \beta_{22} B^2 + \beta_{33} C^2 \quad (3)$$

where Y (%) is the predicted degradation efficiency of dye, β_0 is the interception coefficient, β_1, β_2, and β_3 are linear coefficients, β_{11}, β_{22}, and β_{33} are interaction coefficients, and A (contact time), B (catalyst dosage), and C (pH) are independent variables. The developed quadratic model of the photocatalytic degradation process of malachite green dye in aqueous solution in terms of coded factors is governed by:

$$Y = 72.00 + 12.50\,A + 0.6250B + 19.38\,C - 1.25AB + 6.25AC - 5.00\,BC - 6.00A^2 + 0.2500B^2 - 7.25C^2 \quad (4)$$

Experimental design helps to improve performance characteristics and minimizes error with the minimum number of runs [46]. Table 6 describes the experimental design points used in the matrix of experiments. Also, according to BBD, numbers of seventeen runs were generated based on the interaction of the three variables, as displayed in Table 6.

The lack of fit, regression coefficient (R^2), and Fisher test value were used to confirm the suitability of the anticipated model using analysis of variance (ANOVA) (F-value), and the model was projected as a 3D graph to generate a surface response. Table 7 shows the detailed findings of the quadratic model fitting in ANOVA analysis. The high model Fisher (F) value (78.38) and low p values (<0.0500) demonstrated the model's

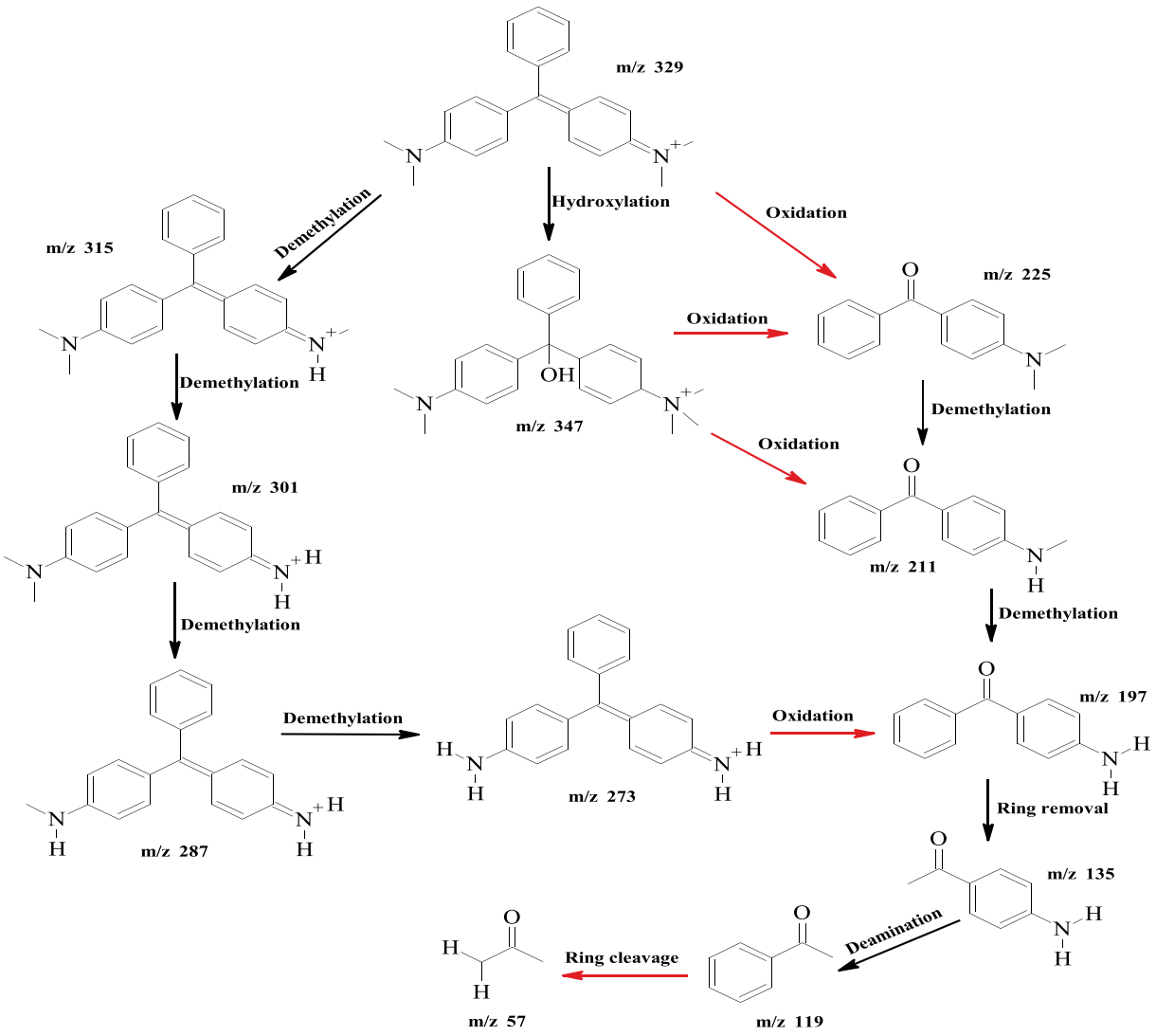

Fig. 17. Proposed reaction pathway of MG degradation.

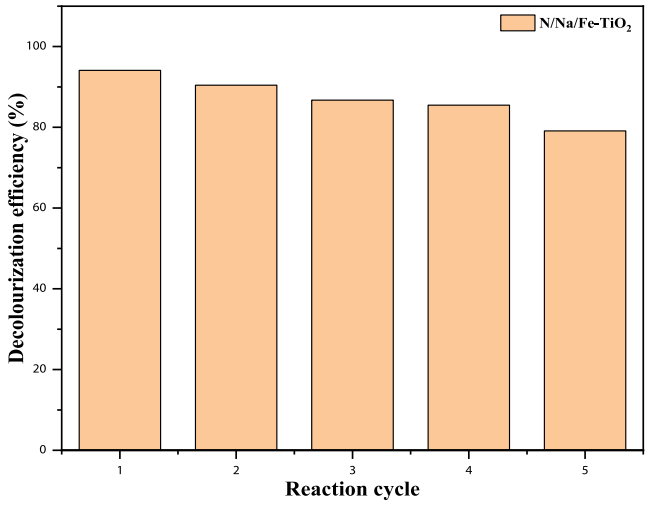

Fig. 18. Effect of Reusability of N/Na/Fe-TiO_2 nanocatalyst photocatalytic degradation of Malachite green dye under optimum operational conditions.

relevance. Because a p-value (Prob > F) <0.05 indicates statistically significant model terms, the model's corresponding p-value (0.0001) indicates that the model is significant [55]. When comparing the F values of interactive model terms, AC had the highest F value of 22.44, showing that the interaction of AC was the most important in MG photodegradation. Furthermore, the Pred. R^2 of 0.9301 was in reasonable agreement with the Adj. R^2 of 0.9775, indicating that the model is reasonably predictable and that the predicted and experimental values are closely related [25,54].

Fig. 13(a) and (b) show a plot of anticipated vs experimental values and a plot of the normal probability of residuals (b). The actual values were close to expected values, indicating adequacy and importance. To further establish validity, the normal probability of the residuals plot was calculated for degrading responses. As can be seen, most of the data points were dependably distributed on a straight trend line, and none of the individual residuals surpassed the residual variance, implying that the degradation regression model used for degradation was adequate [12].

Response surface plots show the interaction between factors and can be used to improve photocatalytic treatment efficiency [19]. Fig. 14 depicts reaction time (A) and catalyst dose (B) effects. Because of the increased amount of photon absorption on the catalyst surface on the nanocatalyst surface, the degree of degradation of malachite green dye increased slowly with increasing catalyst dosage and reached a

maximum of about 0.2 g. The observed effect can be connected to triggering light penetration into the suspension, which increases deterioration efficiency. Additionally, a more noticeable increase was accomplished with an enhanced reaction time due to the availability of more vacant locations. A similar observation was made by Salarian et al. [40].

The efficiency of MG degradation rises with increasing reaction time and pH value, as seen in Fig. 15. The degradation efficiency increases with an increase in pH, as shown in the contour plot. This impact is more noticeable when the catalyst dosage is modest. This can be explained by the photocatalyst's surface charge characteristics. In acidic media, the N/Na/Fe-TiO_2 surface was positively charged. The number of negatively charged sites grows as the pH of the solution rises. Based on electrostatic attraction, this promotes the adsorption of MG (a cationic dye).

The simultaneous effects of pH and catalyst dosage are shown in Fig. 16. pH played a prominent role because the degree of degradation increased exponentially with increasing pH, while catalyst dosage has little effect on the degradation rate. The low initial degradation rate could be due to increased active sites. However, when all dye molecules become absorbed on the photocatalyst surface, a further rise in the photocatalyst dosage exerted little effect on the degradation efficiency.

Optimization and validation over N/Na/Fe-TiO_2 nanocatalyst

The best combination of independent factors that led to the best degradation of dye molecules in an aqueous solution was predicted using the fittest quadratic model. By configuring all of the independent variables of the nanocatalyst tested to be in the range of reaction time, the optimization function of design expert software was utilized to estimate the optimum response (5–30 min), catalyst dosage (0.1–0.2 g) and pH (3–10) and the response (% degradation) set at maximum with 95 % confidence level. The desirability function approach was used to obtain each catalyst's optimized conditions.

At a dopant dosage of 0.11 g, a contact time of 25.38 min, and a pH of 9.89, the photodegradation of MG was 97.89 %, with high desirability of 1. An additional experiment was conducted under the suggested ideal conditions, and the photodegradation of MG was 96.57 %, which was very near to the predicted findings with less than a 2 % difference [21]. Compared with previous literature (see Table 8), the result confirmed that using N, Na, and Fe tri-doped TiO_2, a higher percentage of dye removal can be obtained with a small amount of nanocatalyst. This is in line with earlier research that suggests the validity of RSM for experimental modifications due to its precise predictability [37,40].

MG dye degradation

GC–MS was employed to determine the breakdown products of MG dye decolourization under visible light irradiation and presented in Fig. 17. MG dye molecule was extensively degraded after 30 min under visible light irradiation. The active species (hydroxyl radical) from TiO_2 nanocatalysts are extremely reactive species that attack most organic molecules due to oxidation and play a significant role in MG degradation. Some intermediates generated such as 4,4-(dimethylamino) phenyl](phenyl)methylidene (m/z = 315), 4-(dimethylamino)phenyl (m/z = 301), 4-(methylamino) benzophenone (m/z = 211), 4-(dimethylamino) benzophenone (m/z = 225), 1-(4-aminophenyl)ethan-1-one (m/z = 135) and 1-phenylethan-1-one (m/z = 119) were detected. It was proposed that hydroxylation, demethylation, oxidation, deamination, and deformation of benzene due to ring cleavage occurred during the photocatalytic degradation of MG. The photodegradation pathway of MG dye using N/Na/Fe-TiO_2 supported the proposed pathway studied by Barapatre et al. [8]. In this study, the final product (propan-2-one) with a molecular weight of 57 g/mol was detected via the benzene ring cleavage action of 1-phenylethan-1-one. Thus, a series of intermediate products were degraded, which caused the benzene rings to open, forming simple, less toxic molecules. Further degradation could lead to complete mineralization. This is the first study that reported the degradation of MG dye using N/Na/Fe-TiO_2 nanocatalyst.

Recyclability studies

Fig. 18 shows the result of the catalyst reusability and stability tests. During the photocatalytic destruction of organic pollutants, the life lifetime of a photocatalyst is a significant component. The photocatalytic degradation process was experimented with under the optimum conditions of 0.11 g catalyst dose, 25.83 min reaction time, and pH 9.89 dye solution. The photocatalyst was utilized for five reaction cycles, with dye removal efficiencies of 94.10 %, 90.44 %, 86.73 %, 85.49 %, and 79.10 % for each cycle, respectively. N-Na-Fe-TiO_2 nanocatalyst revealed significant photostability without any substantial loss in photocatalytic activity even up to the fifth cycle, which could indicate the good physicochemical stability of the synthesized N/Na/Fe-TiO_2 by the hydrothermal assisted green synthesis method. As reusability increases, the observed photodegradation efficiency decreases, which could be attributed to fewer active sites for adsorption. In addition, intermediates were produced during the photocatalytic breakdown of the dyeing effluent [42]. Because these species may be adsorbed on the catalyst's surface, the number of reaction species ($OH^{\bullet}$ and $O_2^{\bullet}$-) required for dye degradation increases [53]. As a result, the available OH radicals are insufficient to degrade the dye in subsequent reactions. As a result, as the used catalyst is re-used, the dye degradation efficiency drops. Furthermore, delayed mass transfer of produced intermediates from the catalyst surface can result in the deactivation of the N/Na/Fe-TiO_2 active sites and, as a result, decrease decolourization efficiency.

Conclusion

In summary, a highly efficient and eco-friendly approach was adopted to synthesize N-Na-Fe-TiO_2 nanoparticles through a hydrothermal-assisted green synthesis route. The nanoparticle materials were characterized with XRD, HRTEM, FTIR, XPS, and UV–visible absorption spectroscopy, and the photocatalytic activities of the nanomaterials were evaluated on malachite green dye in an aqueous solution. The UV–vis spectra revealed that the absorption edges of doped samples are significantly red-shifted, which extended to the visible spectrum, owing to the impurity band formation of the above valence band by doping N. The photocatalytic efficiency of undoped and modified TiO_2 followed the sequence: N-Na-Fe-TiO_2 > N-Fe-TiO_2 > Na-TiO_2 > TiO_2. The recycling study indicated that the photocatalytic efficiency of MG dye using N-Na-Fe-TiO_2 can still reach 79 % after its five cycles, further exhibiting excellent stability and reusability.

CRediT authorship contribution statement

A.T. Amigun: Conceptualization, Methodology, Software, Writing – original draft, Software, Validation, Writing – review & editing. **F.A. Adekola:** Writing – original draft, Visualization, Investigation, Supervision, Software, Validation, Writing – review & editing. **J.O. Tijani:** Writing – original draft, Visualization, Investigation, Software, Validation, Writing – review & editing, Software, Validation, Writing – review & editing. **S. Mustapha:** Writing – original draft, Visualization, Investigation, Software, Validation, Writing – review & editing.

Declaration of Competing Interest

The authors declare that they have no known competing financial interests or personal relationships that could have appeared to influence the work reported in this paper.

Data availability

The data that has been used is confidential.

References

[1] N. Aboualigaledari, M. Rahmani, A review on the synthesis of the TiO_2-based photocatalyst for environmental purification, J. Comp. Comp. 3 (6) (2021) 25–42.

[2] S.M. Adyani, M. Ghorbani, A comparative study of physicochemical and photocatalytic properties of visible light responsive Fe, Gd and P single and tri-doped TiO_2 nanomaterials, J. Rare Earths 36 (1) (2018) 72–85.

[3] N. Ajmal, K. Saraswat, M.A. Bakht, Y. Riadi, M.J. Ahsan, M. Noushad, Cost-effective and eco-friendly synthesis of titanium dioxide (TiO_2) nanoparticles using fruit's peel agro-waste extracts: characterization, in vitro antibacterial, antioxidant activities, Green Chem. Lett. Rev. 12 (3) (2019) 244–254.

[4] W. Anku, S.-O.-B. Oppong, S.K. Shukla, P.P. Govender, Comparative photocatalytic degradation of monoazo and diazo dyes under simulated visible light using Fe^{3+}/C/S doped-TiO_2 nanoparticles, Acta Chim. Slov. 63 (2) (2016) 380–391.

[5] B. Appavu, S. Thiripuranthagan, Visible active N, S co-doped TiO_2/graphene photocatalysts for the degradation of hazardous dyes, J. Photochem. Photobiol. A-Chemistry 340 (2017) 146–156.

[6] Y. Aristanti, Y. Supriyatna, N. Masduki, S. Soepriyanto, Effect of calcination temperature on the characteristics of TiO_2 synthesized from ilmenite and its applications for photocatalysis. Paper presented at the IOP Conference Series: Materials Science and Engineering, 2019.

[7] R. Bagheri, M. Ghaedi, A. Asfaram, E.A. Dil, H. Javadian, RSM-CCD design of malachite green adsorption onto activated carbon with multimodal pore size distribution prepared from Amygdalus scoparia: Kinetic and isotherm studies, Polyhedron 171 (2019) 464–472.

[8] A. Barapatre, K.R. Aadil, H. Jha, Biodegradation of malachite green by the ligninolytic fungus Aspergillus flavus, CLEAN–Soil, Air Water 45 (4) (2017) 1600045.

[9] N. Chauhan, V. Singh, S. Kumar, M. Kumari, K. Sirohi, Synthesis of nitrogen & palladium co-doped mesoporous titanium dioxide nanoparticles via evaporation induced self assembly method and study of their photocatalytic properties, J. Mol. Struct. 1185 (2019) 219–228.

[10] H.-H. Cheng, S.-S. Chen, S.-Y. Yang, H.-M. Liu, K.-S. Lin, Sol-Gel hydrothermal synthesis and visible light photocatalytic degradation performance of Fe/N co-doped TiO_2 catalysts, Materials 11 (6) (2018) 939.

[11] P. Chowdhary, R.N. Bharagava, S. Mishra, N. Khan, Role of Industries in Water Scarcity and its Adverse Effects on Environment and Human Health Environmental Concerns and Sustainable Development, Springer, 2020, pp. 235–256.

[12] E.A. Dil, M. Ghaedi, A. Asfaram, F. Mehrabi, A.A. Bazrafshan, Optimization of process parameters for determination of trace Hazardous dyes from industrial wastewaters based on nanostructures materials under ultrasound energy, Ultrason. Sonochem. 40 (2018) 238–248.

[13] A. El Nemr, E.T. Helmy, E.A. Gomaa, S. Eldafrawy, M. Mousa, Photocatalytic and biological activities of undoped and doped TiO_2 prepared by Green method for water treatment, J. Environ. Chem. Eng. 7 (5) (2019), 103385.

[14] A.N. El-Shazly, A.H. Hegazy, E. El Shenawy, M.A. Hamza, N.K. Allam, Novel facet-engineered multi-doped TiO2 mesocrystals with unprecedented visible light photocatalytic hydrogen production, Sol. Energy Mater. Sol. Cells 220 (2021), 110825.

[15] E.R. Essien, V.N. Atasie, T.O. Oyebanji, D.O. Nwude, Biomimetic synthesis of magnesium oxide nanoparticles using Chromolaena odorata (L.) leaf extract, Chem. Pap. (2020) 1–9.

[16] S.P. Goutam, G. Saxena, V. Singh, A.K. Yadav, R.N. Bharagava, K.B. Thapa, Green synthesis of TiO_2 nanoparticles using leaf extract of Jatropha curcas L. for photocatalytic degradation of tannery wastewater, Chem. Eng. J. 336 (2018) 386–396.

[17] S. Guan, L. Hao, S. Kasuga, H. Yoshida, Y. Cheng, Y. Lu, Enhanced photocatalytic activity of titania coatings fabricated at relatively low oxidation temperature with sulfate-acid-bath pretreatment, Appl. Phys. A 126 (7) (2020) 1–6.

[18] Y. Huang, C.Y. Haw, Z. Zheng, J. Kang, J.C. Zheng, H.Q. Wang, Biosynthesis of zinc oxide nanomaterials from plant extracts and future green prospects: a topical review. Adv. Sustainable Syst., 2021, 2000266.

[19] S. Kassahun, Z. Kiflie, D. Shin, S. Park, Photocatalytic decolorization of methylene blue by N-doped TiO_2 nanoparticles prepared under different synthesis parameters, J. Water Environ. Nanotechnol. 2 (3) (2017) 136–144.

[20] A. Kumar, D. Kumar, G. Pandey, Characterisation of hydrothermally synthesised CuO nanoparticles at different pH, J. Technol. Adv. Sci. Res. 2 (4) (2016) 166–169.

[21] E. Kweinor Tetteh, E. Obotey Ezugbe, D. Asante-Sackey, E.K. Armah, S. Rathilal, Response surface methodology: photocatalytic degradation kinetics of basic blue 41 dye using activated carbon with TiO_2, Molecules 26 (4) (2021) 1068.

[22] A.B. Lavand, Y.S. Malghe, Synthesis, characterization and visible light photocatalytic activity of carbon and iron modified ZnO, J. King Saud Univ.-Sci. 30 (1) (2018) 65–74.

[23] O. León, A. Muñoz-Bonilla, D. Soto, D. Pérez, M. Rangel, M. Colina, M. Fernández-García, Removal of anionic and cationic dyes with bioadsorbent oxidized chitosans, Carbohydr. Polym. 194 (2018) 375–383.

[24] W. Li, L. Xie, L. Zhou, J. Ochoa-Lozano, C. Li, X. Chai, A systemic study on Gd, Fe and N co-doped TiO_2 nanomaterials for enhanced photocatalytic activity under visible light irradiation, Ceram. Int. 46 (15) (2020) 24744–24752.

[25] Y.P. Lin, M. Mehrvar, Photocatalytic treatment of an actual confectionery wastewater using Ag/TiO_2/Fe_2O_3: optimization of photocatalytic reactions using surface response methodology, Catalysts 8 (10) (2018) 409.

[26] P.A. Luque, H.E. Garrafa-Gálvez, O. Nava, A. Olivas, M.E. Martínez-Rosas, A. R. Vilchis-Nestor, A. Villegas-Fuentes, M.J. Chinchillas-Chinchillas, Efficient sunlight and UV photocatalytic degradation of Methyl Orange, Methylene Blue and Rhodamine B, using Citrus× paradisi synthesized SnO_2 semiconductor nanoparticles, Ceramics 47 (17) (2021) 23861–23874.

[27] A. Mancuso, O. Sacco, D. Sannino, S. Pragliola, V. Vaiano, Enhanced visible-light-driven photodegradation of Acid Orange 7 azo dye in aqueous solution using Fe-N co-doped TiO_2, Arabian J. Chem. 13 (11) (2020) 8347–8360.

[28] M.A. Mannaa, K.F. Qasim, F.T. Alshorifi, S.M. El-Bahy, R.S. Salama, Role of NiO nanoparticles in enhancing structure properties of TiO_2 and its applications in photodegradation and hydrogen evolution, ACS Omega 6 (45) (2021) 30386–30400.

[29] M. Masae, P. Pitsuwan, C. Pholthawon, N. Pawanwatcharakorn, L. Sikong, P. Kongsong, Synthesis of Na doped TiO_2 nano photocatalysts film on its photoactivity and hydrophilicity, Sci. Technol. Asia (2015) 63–71.

[30] A. Mayoufi, M.F. Nsib, O. Ahmed, A. Houas, Synthesis, characterization and photocatalytic performance of W, N, S-tri-doped TiO_2 under visible light irradiation, C. R. Chim. 18 (8) (2015) 875–882.

[31] L. Mino, C. Negri, A. Zecchina, G. Spoto, Photodegradation of organic pollutants on TiO_2 P25 surfaces investigated by transmission FTIR spectroscopy under in situ UV-Vis irradiation, Z. Phys. Chem. 230 (9) (2016) 1441–1451.

[32] A.-T. Mohammad, A.S. Abdulhameed, A.H. Jawad, Box-Behnken design to optimize the synthesis of new crosslinked chitosan-glyoxal/TiO_2 nanocomposite: methyl orange adsorption and mechanism studies, Int. J. Biol. Macromol. 129 (2019) 98–109.

[33] S. Mustapha, J.O. Tijani, M.M. Ndamitso, A.S. Abdulkareem, D.T. Shuaib, A. K. Mohammed, Adsorptive removal of pollutants from industrial wastewater using mesoporous kaolin and kaolin/TiO_2 nanoadsorbents, Environ. Nanotechnol. Monit. Manage. 15 (2021), 100414.

[34] S. Mustapha, J.O. Tijani, M.M. Ndamitso, A.S. Abdulkareem, D.T. Shuaib, A. T. Amigun, H.L. Abubakar, Facile synthesis and characterization of TiO_2 nanoparticles: X-ray peak profile analysis using Williamson-Hall and Debye-Scherrer methods, Int. Nano Lett. 11 (3) (2021) 241–261.

[35] N. Nandhini, S. Rajeshkumar, S. Mythili, The possible mechanism of eco-friendly synthesized nanoparticles on hazardous dyes degradation, Biocatal. Agric. Biotechnol. 19 (2019), 101138.

[36] M.-H. Pham, C.-T. Dinh, G.-T. Vuong, N.-D. Ta, T.-O. Do, Visible light induced hydrogen generation using a hollow photocatalyst with two cocatalysts separated on two surface sides, PCCP 16 (13) (2014) 5937–5941.

[37] M. Pirsaheb, H. Hossaini, R. Nabizadeh, N. Azizi, Zeolite-intermittent cycle moving bed air-lift bioreactor (Zeo-ICMBABR) for composting leachate treatment; simultaneous COD, nitrogen and phosphorous compounds removal, J. Environ. Health Sci. Eng. 18 (2) (2020) 933–945.

[38] K. Rivera, M. De Luna, T. Suwannaruang, K. Wantala, Photocatalytic degradation of reactive red 3 and alachlor over uncalcined Fe–TiO_2 synthesized via hydrothermal method, Desalin. Water Treat. 57 (46) (2016) 22017–22028.

[39] A. Sadeghzadeh-Attar, Photocatalytic degradation evaluation of N-Fe co-doped aligned TiO_2 nanorods based on the effect of annealing temperature, J. Adv. Ceram. 9 (1) (2020) 107–122.

[40] A.-A. Salarian, Z. Hami, N. Mirzaei, S.M. Mohseni, A. Asadi, H. Bahrami, M. Vosoughi, A. Alinejad, M.-R. Zare, N-doped TiO_2 nanosheets for photocatalytic degradation and mineralization of diazinon under simulated solar irradiation: Optimization and modeling using a response surface methodology, J. Mol. Liq. 220 (2016) 183–191.

[41] K. Salehi, B. Shahmoradi, A. Bahmani, M. Pirsaheb, H. Shivaraju, Optimization of reactive black 5 degradation using hydrothermally synthesized NiO/TiO_2 nanocomposite under natural sunlight irradiation, Desalin. Water Treat. 57 (52) (2016) 25256–25266.

[42] R.G. Saratale, G.S. Ghodake, S.K. Shinde, S.-K. Cho, G.D. Saratale, A. Pugazhendhi, R.N. Bharagava, Photocatalytic activity of CuO/Cu (OH) 2 nanostructures in the degradation of Reactive Green 19A and textile effluent, phytotoxicity studies and their biogenic properties (antibacterial and anticancer), J. Environ. Manage. 223 (2018) 1086–1097.

[43] E.B. Simsek, Solvothermal synthesized boron doped TiO_2 catalysts: photocatalytic degradation of endocrine disrupting compounds and pharmaceuticals under visible light irradiation, Appl. Catal. B 200 (2017) 309–322.

[44] S.N.A. Sulaiman, M. Zaky Noh, N. Nadia Adnan, N. Bidin, S.N. Ab Razak, Effects of photocatalytic activity of metal and non-metal doped TiO_2 for hydrogen production enhancement-a review, J. Phys. Conf. Ser. 1027 (2018) 012006.

[45] T. Suwannaruang, J.P. Hildebrand, D.H. Taffa, M. Wark, K. Kamonsuangkasem, P. Chirawatkul, K. Wantala, Visible light-induced degradation of antibiotic ciprofloxacin over Fe–N–TiO2 mesoporous photocatalyst with anatase/rutile/brookite nanocrystal mixture, J. Photochem. Photobiol., A 391 (2020), 112371.

[46] M.G. Tavares, D.H. Santos, M.G. Tavares, J.L. Duarte, L. Meili, W.R. Pimentel, C. L. Zanta, Removal of reactive dyes from aqueous solution by Fenton reaction: kinetic study and phytotoxicity tests, Water Air Soil Pollut. 231 (2) (2020) 1–15.

[47] S. Tichapondwa, J. Newman, O. Kubheka, Effect of TiO_2 phase on the photocatalytic degradation of methylene blue dye, Phys. Chem. Earth, Parts A/B/C 118 (2020), 102900.

[48] J.O. Tijani, O. Ugochukwu, L. Fadipe, M. Bankole, A. Abdulkareem, W. Roos, Photocatalytic degradation of local dyeing wastewater by iodine-phosphorus co-doped tungsten trioxide nanocomposites under natural sunlight irradiation, J. Environ. Manage. 236 (2019) 519–533.

[49] N. Turkten, M. Bekbolet, Doped TiO2 photocatalysts for the photocatalytic degradation efficiency of methylene blue and humic acid under solar light, Hittite J. Sci. Eng. 7 (2) (2020) 109–114.

[50] V. Vaiano, O. Sacco, G. Libralato, G. Lofrano, A. Siciliano, F. Carraturo, M. Carotenuto, Degradation of anionic azo dyes in aqueous solution using a

continuous flow photocatalytic packed-bed reactor: Influence of water matrix and toxicity evaluation, J. Environ. Chem. Eng. 8 (6) (2020), 104549.
[51] W. Xie, R. Li, Q. Xu, Enhanced photocatalytic activity of Se-doped TiO_2 under visible light irradiation, Sci. Rep. 8 (1) (2018) 1–10.
[52] M. Yuan, X. Fu, J. Yu, Y. Xu, J. Huang, Q. Li, D. Sun, Green synthesized iron nanoparticles as highly efficient fenton-like catalyst for degradation of dyes, Chemosphere 261 (2020), 127618.
[53] A.S. Yusuff, I.I. Olateju, O.A. Adesina, TiO_2/anthill clay as a heterogeneous catalyst for solar photocatalytic degradation of textile wastewater: Catalyst characterization and optimization studies, Materialia 8 (2019) 100484.
[54] Z. Zafar, J.-O. Kim, Optimization of hydrothermal synthesis of Fe–TiO_2 nanotube arrays for enhancement in visible light using an experimental design methodology, Environ. Res. 189 (2020), 109908.
[55] H. Zangeneh, M. Farhadian, A.A. Zinatizadeh, A reusable visible driven N and C-N doped TiO_2 magnetic nanocomposites for photodegradation of direct red 16 azo dye in water and wastewater, Environ. Technol. (2020) 1–16.
[56] A. Zhang, Z. Zhang, J. Chen, W. Sheng, L. Sun, J. Xiang, Effect of calcination temperature on the activity and structure of MnOx/TiO_2 adsorbent for Hg^o removal, Fuel Process. Technol. 135 (2015) 25–33.
[57] C. Gaidau, A. Petica, M. Ignat, O. Iordache, L.M. Ditu, M. Ionescu, Enhanced photocatalysts based on Ag-TiO_2 and Ag-N-TiO_2 nanoparticles for multifunctional leather surface coating, Open Chem. 14 (1) (2016) 383–392.
[58] L. Zhao, Y. Xie, Q. Lin, R. Zheng, Y Diao, Preparation of C, N and P co-doped TiO_2 and its photocatalytic activity under visible light, Functional Mater. Lett. 12 (4) (2019) 1950045.